EÖTVÖS LORÁND GEOPHYSICAL INSTITUTE OF HUNGARY
MAGYAR ÁLLAMI EÖTVÖS LORÁND GEOFIZIKAI INTÉZET
ВЕНГЕРСКИЙ ГЕОФИЗИЧЕСКИЙ ИНСТИТУТ ИМ. Л. ЭТВЕША

GEOPHYSICAL TRANSACTIONS
GEOFIZIKAI KÖZLEMÉNYEK
ГЕОФИЗИЧЕСКИЙ БЮЛЛЕТЕНЬ

28/2

BUDAPEST
1982

ETO/UDC 550.3(061.6) (439 Budapest) (058)
HU ISSN 0016—7177

Felelős kiadó: MÜLLER Pál

Manuscripts and all correspondence to:
Editor, Geophysical Transactions, Eötvös Loránd Geophysical Institute
of Hungary, POB 35, Budapest, H-1440, Hungary

CONTENTS

TARTALOM

СОДЕРЖАНИЕ

EÖTVÖS LORÁND GEOPHYSICAL INSTITUTE OF HUNGARY
GEOPHYSICAL TRANSACTIONS 1982
28/2 pp. 5—17

GEOPHYSICAL STUDY OF THE EPICENTRAL AREA OF ALKYONIDES ISLANDS EARTHQUAKES, CENTRAL GREECE

M. L. MYRIANTHIS*

During February and March 1981, three strong earthquakes accompanied by a sequence of shocks of lower magnitude occurred in the northeastern part of the Gulf of Corinth near the Alkyonides Islands in Central Greece. This study attempts an appreciation of the causes of earthquakes in the epicentral region. In order to investigate the geotectonic conditions of the broader epicentral area two marine seismic profiles and a number of marine gravity records are examined and presented. Finally, a simplified model is proposed to explain the present morphology of the Gulf of Corinth graben.

Introduction

On 24 and 25 February 1981 a triggering of intense seismic activity occurred taking the form of series of earthquakes in the northeastern part of the Gulf of Corinth, in Central Greece. According to released data by the Geodynamical Institute of Athens Observatory, the first event initiated on 24 February at 20 : 53 : 37 hours GMT, having epicentral coordinates 38° 13′ 5″ N, 23° 0.06′ 00″ E and magnitude $M_s = 6.6$. The shock was strongly felt in Athens with intensity ranging between VI and VII on the Mercalli scale depending on the geomorphological characteristics of the particular area. The main aftershock occurred at 02 : 35 : 36 hours on 25th February. The coordinates of the epicentre were 38° 9′ 0″ N and 23° 8′ 2″ E. The magnitude of this shock was $M_s = 6.2$.

Furthermore, on 4th March a second set of earthquakes initiated at 21 : 58 hours with magnitude $M_s = 6.2$, followed the next day by an $M_s = 5.9$ event. The first shock occurred approximately 20 km to the northeast of the main shock of 24th February [DRAKOPOULOS et al. 1981].

The Gulf of Corinth is a tectonically active area exhibiting considerable seismicity. Earlier researchers have recognized the region as lying in an extensive tectonic environment with the area to the north and northeast and to the south and southwest continuing to be uplifted at a very high rate. The overall effect of this uplift is the formation of the Gulf of Corinth [TILFORD et al. 1981] which is an asymmetric graben. This view is also supported from the bathymetric and topographic features of the area [SABOT and MAROUKIAN 1981].

In 1970 the Gulf of Corinth was for the first time the subject of systematic marine geophysical research designed as a reconnaissance survey for oil exploration purposes. Seismic reflection data of high quality were accordingly acquisitioned and digitally processed.

* Public Petroleum Corporation of Greece S.A. Academias 54, Athens, 143, Greece
Manuscript received (revised form): 20. 7. 1982.

Following the recent intense seismic activity it was thought to interpret two selected profiles passing close to the epicentres of the main shock and the aftershock. However, profile KO—105A southeast to northwest and profile KO—102 trending northeast to southwest were chosen; a longitudinal and transverse section with regard to the axis of symmetry of the Gulf of Corinth.

The present paper attempts to evaluate some of the information available concerning the seismicity and stress regime of the area in the light of the data from seismic reflection profiles.

This is hoped to lead to a better understanding of the prevailing geotectonic state and the processes which finally led to the major earthquakes.

Seismic data acquisition and processing

From 10th to 15th September 1979, on behalf of the Public Petroleum Corporation of Greece, the research vessel M/V WESTERN BEACH conducted an extensive geophysical exploration in the Gulf of Corinth. This survey comprised accurate radionavigation, seismic profiling, gravity recording and precise bathymetry.

The MAXIPULSE system was used as the energy source for the entire survey, at a rate of 40 shots per kilometre.

The 2400 m buoyant oil filled streamer cable was used giving 96×25 m groups with 20 geophones per group.

During operations the cable was streamed at a depth of 11—13 m. A set of six pressure sensitive depth transducers was equally spaced down the cable. Eight cable "depth controllers" were spread down the cable to aid in maintaining the cable at the desired running depth. The distance from the Syledis navigation antenna to the centre of group 96 was 202.75 m and the distance from the Syledis navigation antenna to the gun was 44.53 m. Data from the survey were recorded using an LRS 888 digital seismic recording system.

A minimum of 6.0 s of data was recorded at a 4 ms sampling rate. Input signals to the A/D converter as well as the tape output were continuously monitored on an oscilloscope. An uncorrected 100% shipboard section was also recorded.

The recording filter settings used during this survey were the Low-Cut 6 Hz and the Hi-Cut 87.50 Hz.

Seismic data were processed at the London Data Processing Centre of Western Geophysical Company.

Initially, field data were demultiplexed from scan sequential order to trace sequential order. The bubble sequence, taken from channel 98 of each file, was searched for time-break and the file time adjusted to compensate for the variation in digital start-to time-break inherent in the MAXIPULSE system. From time-break, the first 512 ms of the bubbie sequence was used to design a Wiener—Levinson least squares error filter operator (992 ms long) which, when convolved with the bubble sequence, would produce a single sample negative spike. This operator was convolved with each input data trace to produce the

output data trace. A unique operator was computed for each file. Input, computation and output were in 32 bit floating point mode at a 4 ms sample rate.

A zero-phase bandpass filter of 6 Hz (12 dB/oct) low-cut was also applied before deconvolution.

A Wiener—Levinson least squares predictive deconvolution filter was computed from and applied to the data on a trace by trace basis. The filter operator was computed from the autocorrelation of the input trace and the specified minimum predictive lag.

The deconvolution parameters selected for the Gulf of Corinth area are presented in *Table I*.

Table I

DECONVOLUTION PARAMETERS

MODE OF DECONVOLUTION	NUMBER OF WINDOWS	WINDOW LENGTH (ms)	LENGTH OF OPERATOR (ms)	MINIMUM PREDICTIVE LAG (ms)
BEFORE STACK	2	2200	248	12
AFTER STACK	1	4000	220	40

A multiple attenuation filter (MAF) was applied to the deconvolved CDP output of the preprocessor program before running velocity analyses.

In the MAF, traces within a CDP were NMO corrected with a velocity of 1550 m/s to align the strong, low velocity, multiple energy. A model trace was constructed by summing traces near to, but excluding, the trace to be filtered. From the time of the first water bottom multiple, the model trace was subtracted from the input trace and the process proceeded trace by trace continually within each CDP. Inverse NMO was then applied.

Velocity analyses were performed using the VELAN program on the output of the MAF program.

Stacking velocities were obtained from the interpretation of the VELAN.

Filter pass-bands as specified on each section were applied to the data at the times indicated. Pass-bands at intermediate times were linearly interpolated to give a smooth, gradual transition between specified filters. The time positions of the filters were varied according to structure.

Interpretation of seismic reflection profiles

The 21 km long profile KO—102 runs generally northeast—southwest revealing a well defined asymmetric graben, as shown in *Fig. 1*. Seven kilometres from the northern end of the section in the same direction of shooting lies the epicentre of the main earthquake of 24th February 1981. This part of the profile is governed by a strong shallow reflector developed in some places on the sea bottom in water depths of approximately 330 m. The horizon in question is considered as the basement and is attributed to the top of Mesozoic in general and most probably to Triassic. Lithologically it consists of limestone and dolomite.

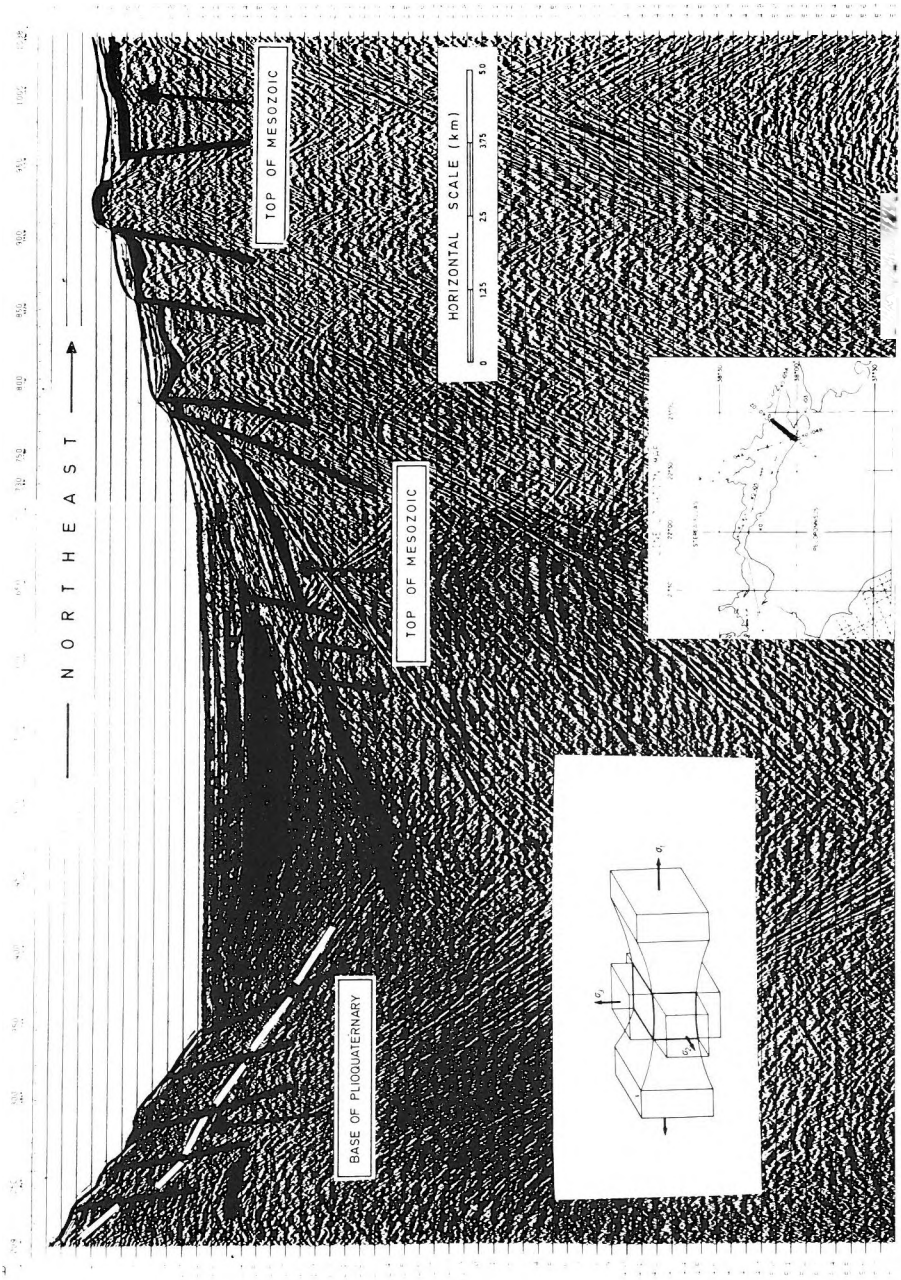
NORTHEAST
TOP OF MESOZOIC
TOP OF MESOZOIC
BASE OF PLIOQUATERNARY
HORIZONTAL SCALE (km)
0
125
25
375
50

Fig. 1. Seismic reflection profile KO—102 crossing the Gulf of Corinth asymmetrical graben. The lower left corner shows a rock mechanical analogy of a rod subject to tensile triaxial stress. Note that in Dreyer's experiment the relationship between the biaxial stress field $\sigma_2 = \sigma_3$ and σ_1 is $\sigma_2 = \sigma_3 > \sigma_1$

1. ábra. A Korinthoszi-öböl aszimmetrikus árkát keresztező KO—102 szeizmikus reflexiós szelvény. A bal alsó sarokban háromtengelyű húzási feszültségnek kitett rúd kőzetmechanikai analógiája látható. Megjegyzendő, hogy a Dreyer-kísérletben a kéttengelyű feszültség-tér $\sigma_2 = \sigma_3$ és σ_1 közötti összefüggés: $\sigma_2 = \sigma_3 > \sigma_1$

Фиг. 1. Профиль сейсморазведки МОВ КО-102, пересекающий асимметричный грабен Коринфского залива. В левом нижнем углу — схема механических деформаций стержня под воздействием трехосевого растяжения. Следует отметить, что в экспериментах Дрейера по двухосному растяжению имело место $\sigma_2 = \sigma_3 > \sigma_1$.

This unit which is widespread in the area geotectonically belongs to the west side of the Pelagonic ridge. Overlying the basement there are some strong reflector seismic facies of limited extent and thickness which could be assigned to Parnassian flyschoid. They were recognized by CLEMENT [1977] in the southern Beotian zone where the northeastern end of profile KO—102 terminates near the little island of Phonias. The general basement structure is controlled by step-faulting. There is also evidence of toe slumping of the sediments overlying the basement* dipping to the southwest forming the acoustic basement of the sedimentary basin. In the southern flank of the graben there is little evidence of the basement which appears sporadically below chaotic depositional patterns. However, a basement reflection is recognizable at 1.3 s suggesting the existence of a large normal faulting system striking east—west and dipping to the northeast. The approximate throw of the fault is estimated to 1500 m. Onshore geological data from the Parachora area support the existence of parallel fault zones running east—west along the northern slope of the Gerania Mountains on the Perachora—Alepochori axis, as shown in *Fig. 2.*

As can be seen from *Figs. 1* and *2*, there is little ambiguity that this large normal fault is the offshore extension of the long normal fault of the Perachora—Alepochori axis. It is interesting to realize that the same fault is considered as the cause of the main earthquake of 24th February 1981. Thus, PAPAZACHOS et al. [1981] argue that the first two earthquakes are due to a normal fault which dips to the north and strikes parallel to the Gulf of Alkyonides as illustrated in *Fig. 2.* Field geophysical data reported by DRAKOPOULOS et al. [1981] revealed two surface ruptures each of 9 to 12 km in length trending east—west. These features are also created by earthquakes which occurred in February 1981 near the Alkyonides Islands. Movement was down to the north on both traces and a total vertical offset of up to 1.5 m has been measured. The preliminary composite local mechanism solution indicates that most of the activity occurs along east—west normal faults.

Sesmic profile KO—102 indicates the presence of another reflector overlying the basement. This horizon is clearly shown in the southern part of the graben. Geologically it is attributed to the base of Plio—Quaternary. Land data in the area of Corinth and Kiato suggest the existence of sand, clay, marls, conglomerates; rarely limestone, gypsum and lignites.

* A strong reflection package which is attributed to a carbonate surface.

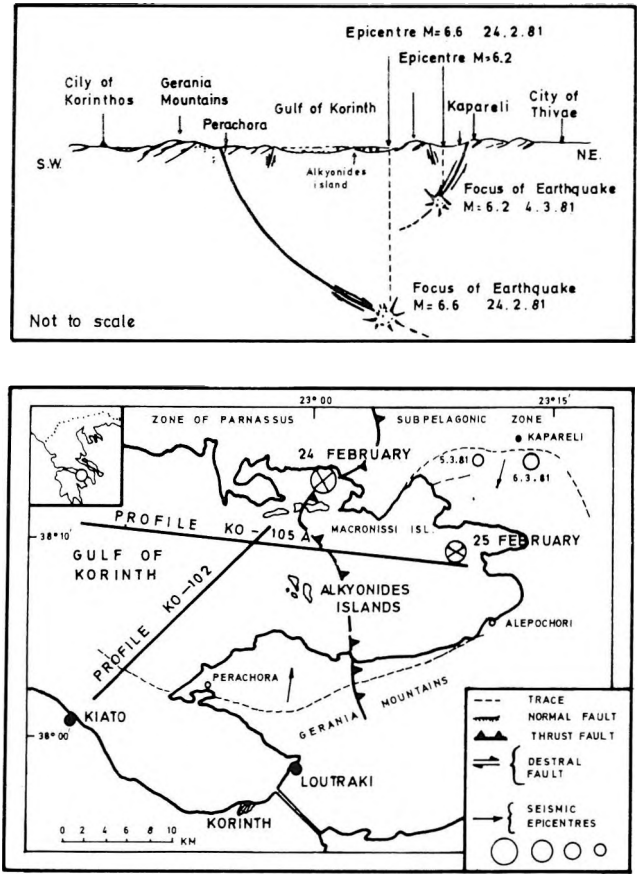

Fig. 2. Above: A schematic section of the epicentral area of the February and March 1981 earthquakes in the Alkyonides islands, Gulf of Corinth. (After PAPAZACHOS et al. 1981)
Below: Generalized location map of the epicentral area. Marine seismic profiles are included as well as the inferred thrusted fault. (Modified from PAPAZACHOS et al. 1981)

2. ábra. Fent: az 1981. február—márciusi földrengések epicentrális területének vázlatos szelvénye (PAPAZACHOS et al. 1981 után)
Lent: az epicentrális terület általánosított helyszínrajza, a tengeri szeizmikus vonalak és a javasolt feltolódási vonal feltüntetésével (módosítva PAPAZACHOS et al. 1981 után)

Фиг. 2. Вверху: схематический профиль зоны эпицентров землетрясений в феврале—марте 1981. г. (по PAPAZACHOS et al., 1981). Внизу: обобщенный схематический план ситуации зоны эпицентров с обозначением линий морской сейсморазведки и предполагаемого взброса (по PAPAZACHOS et al., 1981., с изменениями).

These sediment are mostly freshwater but there also exist brackish and salt-water deposits all of Pliocene age. The seismic section reveals a noticeable, although gentle, relief on the base of Plio—Quaternary involved with diffraction patterns suggesting the presence of closely spaced minor normal faults emerging up to the sea bottom. This is an additional strong indication of active tectonism

which is postulated for the said area from known past strong earthquakes of cumulative magnitudes in the range of $6.0 \leqq M_s \leqq 6.4$.

The Plio—Quaternary reflector is not traceable above the basement in the centre of the elongated asymmetric basin. Structurally, this basin comprises acoustically well stratified laminated reflectors forming a gentle depression. The reflection profile indicates bending of these horizons but not fracturing. This is probably due to the age of the basin and the burial under deep sea conditions, i.e. water depth 800 m. Geometrical elements of the basin indicate a width of approximately 10 km and maximum sedimentary thickness of about one kilometre. Stratigraphy is not known because seismic profiles lack borehole calibration.

In the northeastern edge of the basin sedimentary sequences pinch-out against the basement while in the southern margin seismic records form an angular unconformity with the base of the Plio—Quaternary. The structural difference between the two walls of the graben and the existence at both sides of rather recent normal faulting subparallel to the trend of the basin indicate a differential uplift of these two blocks. The southern one is apparently more active and is undergoing deformation moving upwards with, probably, a higher rate than the northern block.

The 45 km long seismic profile KO—105A runs practically southeast to northwest. As illustrated in *Fig. 3* the eastern end of the section is governed by a proximal onlap environment marking the lateral ending of depositional features. There is evidence of thinning westwards of the relevant seismic units against the reflector assumed to be the top of Mesozoic. Seismic depositional sequences of the area could be divided from the sea bottom to the reflector assigned as the base of the Plio—Quaternary, the second from the said reflector to the horizon representing the top of the Mesozoic. Where both horizons are present they generally run parallel. However, in the central and western part of the profile the Mesozoic basement crops out directly into the sea bottom forming a small sea mountain. The area to the east of this mountain is governed by intense normal faulting. Some normal faults extend deep into the Mesozoic sequence, but they do not continue into the Plio—Quaternary deposits above.

The most distinctive feature of the seismic profile KO—105A appears near the epicentre of the main earthquake of 24th February 1981. The tectonic frame of this area suggests thrust faulting passing virtually through the epicentre. Land geological mapping indicates an overthrust of the subpelagonic on the Parnassos geotectonic zone.

Delineation of the overthrust in provided by various authors notably CLÉMENT [1977]; this latter author suggests that the actual line passes in the north (Sterea Hellas) from the Elopia—Korombili axis in Beotia through the Gulf of Domvraina and between the Makronissi and the nearby small islands probably continuing offshore east of Alkyonides Islands and finally terminating at the Gerania Mountains to the south (see Fig. 2).

The same delineation although on a considerably larger scale is adopted by THIÉBAULT [1977], while FLEURY [1980] accepts in principle the above picture arguing that the actual overthrust is between the subpelagonic and Beotian zone.

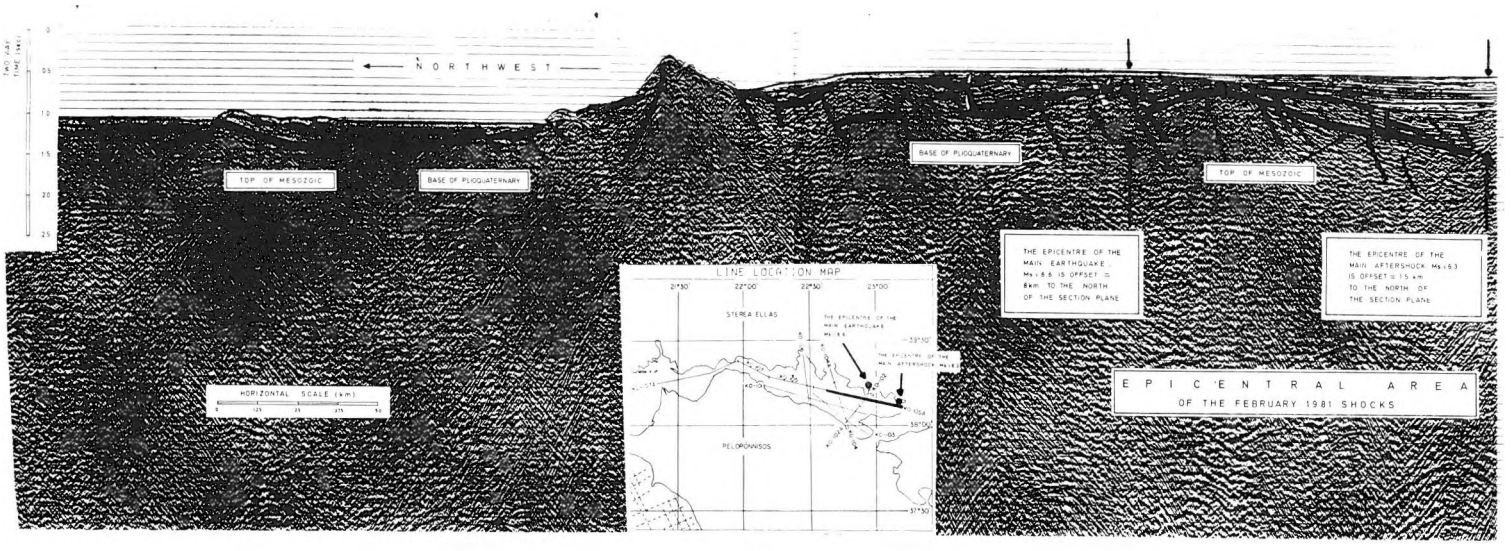

Fig. 3. Reflection profile KO—105A running parallel to the longitudinal axis of the Gulf of Corinth graben. Note that the epicentre of the main earthquake of 24th February 1981 is displaced 8 km to the north of the section plane. As shown, this plane passes through a thrusted fault zone which is assigned (see text) to the overthrust of the sub-Pelagonic on the Parnassos geotectonic zone

3. ábra. A Korinthoszi-öböl tengelyével párhuzamosan futó KO—105A reflexiós szelvény. Az 1981. február 24-i főrengés epicentruma a szelvény síkjától 8 km-re É-ra esik. A szelvény síkja keresztezi azt a feltolódást, amely során a szub-Pelagoniai tektonikai zóna rátolódik a Parnassos zónára

Фиг. 3. Профиль сейсморазведки МОВ КО-105А, параллельный оси Коринфского залива. Эпицентр главного толчка 24-го февраля 1981. г. находится в 8 км к северу от плоскости профиля. Профилем пересекается взброс, по которому Субпелагоническая тектоническая зона надвигается на Парнасскую зону.

The latter zone is thrusting against that of Parnassos. The existence of the inferred Beotian zone which according to CLÉMENT, op cit, appears in the southern part of Sterea Hellas as a flyshoid continuously overlying the Tertiary Parnassian flysch does not alter the main concept that the actual overthrust occurs between the subpelagonic and Parnassos zone. Apparently to the south a buffer zone exist which is the so-called Beotian zone.

Finally, referring to the seismic section shown in Fig. 3, it might be argued that the sea bottom differs morphologically on both sides of the sea mountain. The eastern side represents a relatively calm environment with rather flat bottom at 300 to 312 m water depth. The western side is displaced by a considerable normal fault. Water depths in the eastern sector range between 500 and 800 m.

Gravity recording

Gravity recording was done concurrently with seismic operations. Measurements during the survey were carried out with a LaCoste and Romberg sea gravity meter. The compiled Bouguer anomaly map given in *Fig. 4* provides a comprehensive picture for the Gulf of Corinth area. Calculations are based on a density value of 2.25 g/cm^3.

The trend of the gravity contour lines is NW—SE parallel to the longitudinal axis of the Gulf of Corinth. The values are positive ranging from +80 mgal* in the western extreme of the gulf near the area of Egion in Peloponnese to +125 mgal* in the area of Perachora and the Alkyonides Islands. A rather characteristic feature of the gravity field is the rapid change of the gradient and the observed small local anomaly trending NNW—SSE, i.e. roughly from the area of Corinth to Mount Helicon. This trend is parallel to the main geological and morphological zones of Greece.

Evidently, the trend coincides with a major tectonic event delineating the internal to external geotectonic zones of Greece. The latter zone is associated with the Alpine geosyncline, the westward limit of the internal zone coincides with the sub-Pelagonian zone. Higher values of Bouguer anomalies are expected in this zone due to the presence of ophiolites. MAKRIS [1977], in a detailed geophysical study of Greece, points out that both the mainland and the Peloponnese show negative Bouguer anomalies with maximum negative values of −140 mgal confined to the Ionian and Gavrovo zones of the miogeosynclinal area of the western Hellenides. The gravity field rapidly changes to positive values at the Pelagonian zone. This area has its maximum values at south Attica (+100 mgal). These findings are generally in agreement with the records along the Gulf of Corinth (see *Fig. 4*).

Additionally, it could be argued that the rapid increase eastwards of the gradient of the Bouguer anomalies may be attributed to the inferred overthrust of

* These values are valid as relative differences only because no tie to an accurately defined land gravity station was attempted before the initiation of the survey. However, it is believed that a systematic shift of +30 mgal exists in all measurements. Accordingly the above values are modified to +50 and +95 mgal respectively.

the sub-Pelagonic zone on the Parnassos one. As already shown, delineation of this overthrust was attempted by various authors while the seismic section KO—105A clearly indicates its existence.

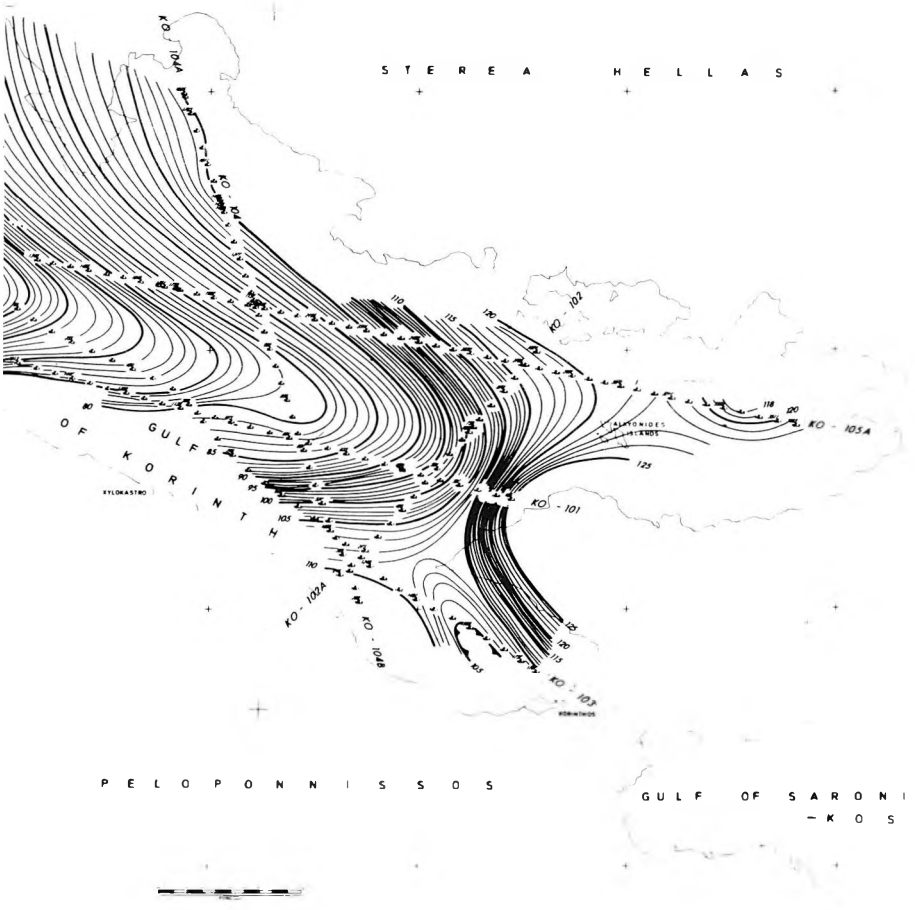

Fig. 4. Bouguer gravity map of the Gulf of Corinth area. The trend of gravity anomalies is NW—SE parallel to the longitudinal axis of the gulf

4. ábra. A Korinthoszi-öböl Bouguer-anomália térképe. Az anomáliák trendje ÉNy—DK, párhuzamosan az öböl hosszanti tengelyével

Фиг. 4. Карта аномалий Буге Коринфского залива. Аномалии вытянуты в СЗ-ЮВ направлении параллельно продольной оси залива.

Seismotectonic regime in the Gulf of Corinth

Bearing in mind the tensile stress regime existing in the Gulf of Corinth ascertained by various authors it might be argued that the Mesozoic formations, which are the basement of the graben shown in the seismic profile KO—102 (see *Fig. 1*), can be modelled by a rod subject to tensile triaxial state of stress. This is of course an oversimplification. DREYER [1973] describes an axis symmetrical tension experiment where a biaxial stress state $\sigma_2 = \sigma_3$ was superimposed on the tension σ_1 which acted parallel to the rod axis as shown in the left part of *Fig. 1*. This was accomplished experimentally by means of a resin bond. Under uniaxial loading, fracture occurred across the small sample cross-section normal to σ_1. Under multiaxial loading a higher tensile stress up to a maximum σ_{max} value is required to induce failure. In certain specially shaped samples, the fracture plane did not lie in the smallest cross-section but rather it moved towards the margin of the axis-symmetrically stressed region. The strength in the centre portion of the specimen has increased.

Comparison between the real state of stress and the one described in the mechanical model leads to the assumption that the direction of axis σ_1, coinciding with the tensile axis *T* minor principal stress component, is nearly horizontal and strikes north to south. The vertical stress component σ_3 ($\sigma_3 = \sigma_2 > \sigma_1$) coincides with the vertical major principal stress component (axis *P*). As a result both flanks of the graben retain to some degree the original cross-section while the central part undergoes reduction in the cross-section combined with some degree of rock strengthening. Additionally, the observed *(Fig. 1)* major normal faulting at both edges of the graben is consistent with experimentally derived results of the rod where the fracture plane did not lie in the smallest cross-section but where it moved towards the margin. The model also suggests that fracture planes (orthogonal faulting) are normal to the direction of σ_1 which is true as well for the actual case where normal faults strike east—west, normally to the horizontal tensile axis *T*. This axis has a north—south direction. As expected from the model there is apparently no rupture in the basement of the basin itself, i.e. in the assumed smallest cross-sectional area. This is inferred by the gentle folding of the overlying sediments which show no evidence of faulting. The argument is to some extent valid because the state of the sediments reflects the morphology and tectonics of the basement.

The analogy—although generalized—between the state of stress existing in the Corinth graben and the stress and deformational pattern experimentally developed in a rod under triaxial tension is remarkable. A different approach of the problem can be obtained by modern concepts of graben formation based on normal fault mechanisms. A fundamental prerequisite is again the crustal tension.

Conclusions

Seismic reflection profiles along and across the Gulf of the Corinth graben were studied together with marine gravity data. Using a knowledge of the areal geology the ages of the main reflectors are determined as accurately as possible, and the inferred stratigraphy of both seismic sections is interpreted. The obtained results support the already expressed view that the main shock of $M_s = 6.6$ on the Richter scale was due to a large normal fault running east—west and dipping to the north. The first order aftershock of $M_s = 6.2$ was due to an antithetic normal fault running also east—west and dipping to the south. Both normal faults are related to the Corinth graben.

Various studies and seismic reflection results point to the fact that a tensional stress regime prevails in the area. A seismic section across the graben reveals an analogy—as far as stresses and deformations are concerned—to an experimental model consisting of a resin rod subject to tensile triaxial state of stress. However, the direction of the minor principal stress component coincides with the tensile axis *T* which is nearly horizontal and strikes north to south. The major principal stress which is the vertical stress component coincides with the compressional axis *P*.

Acknowledgements

Thanks are due to Professor K. Zachos, Chairman of the Board of the Public Petroleum Corporation of Greece (DEP) S.A, for permission to publish this paper.

Assistance offered on various occasions by Mr. Stathis Chiotis of the Geophysical Department, DEP, is sincerely appreciated.

It should be noted that the opinions expressed in the paper are those of the author alone; they do not necessarily reflect the views of DEP.

REFERENCES

CHEMET, B. 1977: Relations structurales entre la zone du Parnasse et la zone Pélargonienne en Béotie (Grèce continentale). Proc. VI Coll. on the Geol. of the Aegean Region, Vol. 1, pp. 237—251.

DRAKOPOULOS, J., DELIBASIS, N., MAKROPOULOS, K., LOUIS, J., DOLOGLOU, E., KOUSKOUNA, B. 1981: Field geophysical studies associated with the February—March 1981 earthquakes in Central Greece. Abstract submitted to the international symposium on the Hellenic Arc and Trench, Athens, 8—10 April 1981, pp. 135—136.

DREYER, W. 1973: The strength properties of rocks. Part 1 from the Science of Rock Mechanics. Second printing. Trans-Tech Publications, pp. 249—273.

FLEURY, J. J. 1980: Les zones de Gavrovo-Tripolitza et de Pinde-Olonos. Evolution d'une plateforme et d'un bassin dans leur cadre alpin. Societe Geologique de Nord, Vol. I, No. 4, pp. 364—365 et 374—375.

MAKRIS, J. 1977: Seismic and gravity studies in Greece and some geodynamic implications. Proc. VI Coll. on the Geol. of the Aegean Region, Vol. II, pp. 61—85.

MAKRIS, J. 1977: The crust and upper mantle of the Aegean Region obtained from deep seismic soundings. Paper presented at the 15th Gen. Assembly of the E.S.C. Cracow, Poland.

PAPAZACHOS, B., KOMNINAKIS, P., MOUNDRAKIS, D., PAVLIDES, S. 1981: The recent seismic activity in the Gulf of Corinth. Abstract submitted to the international symposium of the Hellenic Arc and Trench, Athens, 8—10 April 1981, p. 134.

SABOT, V., MAROUKIAN, H. 1981: Geomorphology and tectonics in and around the Gulf of Corinth, Greece. Abstract submitted to the international symposium on the Hellenic Arc and Trench, Athens, 8—10 April, 1981, p. 89.

TILFORD, N. R., AMICK, D., CANNON, R., DE BOER, J., SNIDER, F., WILKINSON, S. 1981: Field geological studies on the February—March 1981, earthquakes in Central Greece. Abstract submitted to the international symposium on the Hellenic Arc and Trench, Athens, 8—10 April 1981, pp. 137—138.

THIÉBAULT, F. 1977: Stratigraphie de la série des celeschistes et marbres ("Plattenkalk") en fenêtre dans les massifs du Taygète et du Parnon (Peloponnese—Grèce). Proc. VI Coll. on the Geol. of the Aegean Region, Vol. I, pp. 691—702.

M. L. MYRIANTHIS

AZ ALKYONIDES-SZIGETEK (KÖZÉP-GÖRÖGORSZÁG) KÖRÜLI FÖLDRENGÉSEK EPICENTRÁLIS TERÜLETÉNEK GEOFIZIKAI VIZSGÁLATA

1981 február—márciusában három erős földrengés volt, melyeket egy sorozat kisebb erősségű rengés kísért, a Korinthoszi-öböl ÉK-i részén, az Alkyonides-szigetek közelében. A tanulmány a földrengések kipattanásának okát vizsgálja az epicentrális területen. A tektonikai viszonyok tanulmányozására két tengeri szeizmikus szelvényt és számos tengeri gravitációs felvételt vizsgáltak meg. Végeredményként egy egyszerűsített modellt javasol a Korinthoszi-öböl jelenlegi morfológiájának magyarázatára.

М. Л. МИРИАНТИС

ГЕОФИЗИЧЕСКИЕ ИССЛЕДОВАНИЯ В ЗОНЕ ЭПИЦЕНТРА ЗЕМЛЕТРЯСЕНИЙ Б РАЙОНЕ АЛКИОНИДСКИХ ОСТРОВОВ (СРЕДНЯЯ ГРЕЦИЯ)

В феврале—марте 1981. г. в северо-восточной части Коринфского залива, вблизи Алкионидских островов было три сильных землетрясения, которые сопровождались серией толчков меньшей силы. В работе рассматриваются причины возникновения землетрясений в зоне эпицентров. С целью исследования тектонических условий были изучены два морских сейсмических профиля и ряд материалов морской гравиразведки. В итоге предлагается упрощенная модель для объяснения современной морфологии Коринфского залива.

EÖTVÖS LORÁND GEOPHYSICAL INSTITUTE OF HUNGARY
GEOPHYSICAL TRANSACTIONS 1982
28/2 pp. 19—32

EARTH TIDE OBSERVATIONS WITH RECORDING GRAVIMETER BN—07 (GS—11 No. 190) (1974—1980)

P. VARGA*

Processing is based on a total of 38,136 hourly values (1589 days) collected from 8 different stations. Analysis of earth tide curves permits the inference that the reliability of earth tide parameters obtained corresponds to standards postulated by the literature and the parameters show good agreement with values calculated for theoretical earth models. At the same time a denser network of stations is needed for investigating the areal distribution of these parameters. The accuracy of observations with a single instrument is several tenths of one per cent, nearly equalling the difference between individual stations when measured with the BN—07 gravimeter.

Spectra of residual curves determined by eliminating instrumental drift and lunisolar effect show that a higher accuracy than previously obtained can be achieved with existing instruments when the conditions of observation are improved. A second factor which reduces the reliability of observation results is the inadequate accuracy of gravimeter calibration thereby suggesting the need to study the statistical distribution of micrometer readings.

1. Introduction

The Askania gravimeter type GS—11 No. 190 was furnished with a capacitive sensor by prof. M. Bonatz in 1974 and the modified instrument was designated BN—07. The modification rendered the instrument substantially more suitable for observing earth tides. Here, we present the results of observations that have been performed since the modification, to sum up the experiences and to discuss the trend in areal variations of gravity earth tide parameters, and to deal with two important factors endangering the reliability of observations, namely with systematic effects appearing on the frequencies of earth tides or near them, and with the insufficient accuracy of the calibration of the measuring system.

2. Harmonic analysis of observation series

The observations discussed were performed in the period 1974 through 1980 at eight different stations. The total length of the data system involved in processing is 1589 days (38,136 hours). This data system amounting to approximately 4 years and 4 months is composed of long (405 days at most) and short (90 days at least) partial series. This fact does not allow us to include all the main waves that we detected in the course of the tide analysis, nor to compare the results of individual stations. Our experience, however, suggests that the tidal waves M_2 and O_1

* Eötvös Loránd Geophysical Institute of Hungary
Manuscript received 29. 4. 1982.

can be used reliably even in such instances. For this purpose adequate observation conditions must be created at the stations. The most important factors are the temperature stability of the observation room, the reliability and stability of the electric supply, the adequate accuracy of determining the scales of records [VOLKOV et al. 1976]. With the exception of a single case (Penc) our observations were carried out at stations where, simultaneously with the operation of the BN—07 instrument, other instruments were also being used.

Results of the harmonic analysis of series observed by us in the period 1974—1980 are presented in *Table I*. The effect of world oceans was calculated by PERTSEV [1970] still using the maps compiled by BOGDANOV and MAGARIK [1969], and for the stations Penc and Graz by LICHTENEGGER et al. [1982]. The corrected values of amplitude factors are found in the last two columns of the table. It can be observed that after ocean tide correction the amplitude factors of waves O_1 and M_2 practically agree. Anomalous values were obtained from individual stations. Thus, the amplitude factor M_2 of Obninsk differs from the rest since its corrected value [1,184] exceeds the average by about 2%. The deviation of corrected values is high (1.1%) also in the case of Pecný station. It can be seen from the presented results that in the area investigated by us no regional variations due to geophysical causes of amplitude factors could be detected. In addition to instrumental reasons to be discussed later this can probably be explained by the uneven distribution of the network of our stations. Regional variations of the earth tide parameters must be related to big tectonic structures—causing inhomogeneities in the crust and perhaps in the upper mantle, too. Their assumed position, however, is not followed by the stations.

3. Study of amplitude factors

It is of interest to study the extent of deviations between the amplitude factors of instruments operated at the individual stations and those obtained by the BN—07 gravimeter (GS—11 No. 190). Observations performed within the framework of subproject 14.3 KAPG were subjected to the so called global processing in addition to the usual processing for each instrument [VENEDIKOV 1979]. The essence of global processing is that the observations performed at a given station by individual instruments are mutually adjusted. The amplitude factors and phase differences obtained in this way, as well as the corresponding errors [DITTFELD et al. 1981] are given in the column "GLOBAL" of *Table II* and clearly show the extent to which observations by a single instrument can be regarded as reliable. When these deviations are compared with differences experienced between the individual stations (Table I), the impression is formed that the obtained deviations are of similar order of magnitude. The last line of Table II contains results of the mutual adjustment of all series measured at all stations, at first for BN—07, then for all instruments (see Dittfeld et al. 1981). The O_1 wave obtained using the BN—07 instrument shows good agreement with the values determined from the mutual adjustment of the rest of the instruments whereas for wave M_2 a great deviation (0.6%) can be observed due to the mentioned greater deviation for Obninsk. If this is neglected it can be established that

Station	Length of record (days)	Epoch	Observed amplitude factors		Observed phase differences		Amplitude factors, effect of world oceans eliminated	
			O_1	M_2	O_1	M_2	O_1	M_2
Bonn	90	1974	1.158 ± 3	1.197 ± 3	− 0.55° ± 16	1.92° ± 15	1.165	1.160
Pecný	114	1975	1.159 ± 10	1.181 ± 2	− 0.73° ± 49	1.23° ± 13	1.165	1.154
Obninsk	233	1975—76	1.153 ± 6	1.200 ± 2	− 0.16° ± 30	− 0.31° ± 10	1.157	1.184
Pulkovo	161	1976	1.149 ± 5	1.187 ± 3	− 0.59° ± 25	− 1.20° ± 13	1.154	1.163
Tihany	220	1977—78	1.155 ± 8	1.187 ± 3	0.06° ± 39	0.09° ± 14	1.161	1.161
Potsdam	405	1978—79	1.156 ± 3	1.191 ± 1	0.06° ± 14	1.36° ± 15	1.162	1.164
Penc	122	1979—80	1.158 ± 8	1.191 ± 3	− 0.27° ± 33	− 0.30° ± 20	1.164	1.167
Graz	244	1980—81	1.163 ± 4	1.188 ± 1	0.17° ± 20	1.20° ± 7	1.169	1.162
Mean	1589		1.156 ± 2	1.189 ± 3	− 0.21° ± 12	0.50° ± 38	1.162 ± 2	1.164 ± 3

Table I Results of the harmonic analysis of all observations performed with the BN—07 (GS—11 No. 190) recording gravimeter between 1974 and 1980

I. Táblázat A BN—07 (GS—11 No. 190) regisztráló graviméterrel 1974 és 1980 között végzett összes megfigyelés harmonikus analízisének eredményei

Табл. 1. Результаты гармонического анализа всех наблюдений, произведенных самозаписывающим гравиметром типа БН-07 (ГС-11 № 190) в период 1974 – 1980 гг.

Station	Amplitude factors				Phase differences			
	O_1		M_2		O_1		M_2	
	BN—07	$GLOBAL_1$	BN—07	$GLOBAL_1$	BN—07	$GLOBAL_1$	BN—07	$GLOBAL_1$
Pecný	1.159 ± 10	1.152 ± 2	1.181 ± 2	1.185 ± 1	−0.73° ± 49	−0.19° ± 11	1.23° ± 13	0.73° ± 4
Obninsk	1.153 ± 6	1.158 ± 2	1.200 ± 2	1.190 ± 1	−0.16° ± 30	0.06° ± 10	−0.31° ± 10	−0.16° ± 5
Pulkovo	1.149 ± 5	1.156 ± 3	1.187 ± 3	1.183 ± 2	−0.59° ± 25	−0.30° ± 14	−1.20° ± 13	−0.60° ± 8
Tihany	1.155 ± 8	1.155 ± 3	1.187 ± 3	1.189 ± 1	0.06° ± 39	−0.03° ± 14	0.09° ± 14	0.32° ± 7
Potsdam	1.156 ± 2	1.153 ± 2	1.191 ± 1	1.192 ± 1	0.06° ± 14	−0.25° ± 9	1.36° ± 5	0.81° ± 4
$BN\text{-}07_{GLOBAL}$	1.154 ± 2		1.190 ± 1		−0.06 ± 12		0.54 ± 5	
$GLOBAL_2$		1.152 ± 1		1.184 ± 1		−0.03 ± 5		0.39 ± 2

Table II Comparison of amplitude factors and phase differences obtained by the recording gravimeter BN—07 (GS—11 No. 190) within the scope of the KAPG subproject 14.3 with those determined by the other gravimeters.
In the Table $GLOBAL_1$ indicates the result of the mutual adjustment of all observations at a given station, $GLOBAL_2$ values stemming from the mutual adjustment of all observations at all stations. $BN-07_{GLOBAL}$ indicates the mutual results obtained by the BN—07 instrument at varions stations

II. Táblázat Amplitúdó hányadosok és fáziskülönbségek összehasonlítása a BN—07 (GS—11 No. 190) regisztráló graviméterrel és a többi műszerrel nyert eredmények alapján (a KAPG 14.3 altéma keretében).
A táblázatban $GLOBAL_1$-el jelöltük az egy adott állomáson működött összes műszer együttes kiegyenlítésének eredményét, $GLOBAL_2$-vel pedig az összes állomáson és az összes műszer együttes kiegyenlítéséből adódó értékeket. $BN-07_{GLOBAL}$ a BN—07 műszerrel a különböző állomásokon mért értékek együttes kiegyenlítésének eredményeit jelöli

Табл. II. Сопоставление отношений амплитуд д фазовых смещений на основе результатов, полученных самозаписывающим гравиметром типа БН-07 (ГС-11 № 190) и прочими приборами (в рамках подтемы 14. 3. КАПГ).
В таблице фигурируют следующие условные обозначения:
— результат совместного выравнивания данных по всем приборам, действовавшим на отдельной станции;
— значения, полученные путем совместного выравнивания данных по всем приборам, действовавшим на всех станциях, вместе взятых;
— результаты совместного выравнивания данных, измеренных прибором БН-07 на различных станциях.

for the rest of the stations the difference between the BN—07 and global results is 0.4% or less. In summary it can be stated that the deviations between individual instruments and/or stations are of a similar order and amount to several tenths of one per cent.

4. Residual curves

The geophysical interpretation of the areal variations of amplitude factors makes it necessary to disclose systematic effects on observations performed on individual stations. The so called drift-free residual curves seem to be particularly useful for such investigations. They are calculated in the following manner: at first a theoretical curve — corrected by the real amplitude ratio and phase value — is deduced from the observed one, then the instrument drift is eliminated by linear filtering.

The residual curves were subjected first to statistical analysis. On the basis of the χ^2 test their distribution cannot be regarded as normal even for a low reliability level. This statement is readily illustrated in *Fig. 1*, where distribution curves calculated from the three residual series and the related Gaussian normal distribution are shown as an example. It follows from the significant deviation from the normal distribution that the residual curves cannot be regarded as random because they contain deterministic components. (The following three series were used in the investigation: a 112-days' and an 80-days' long section of the observation at Tihany, and 71 days of the 233-days' long observations at Obninsk.) The amplitude spectra of the residual curves were determined to obtain the systematic components. *Figure 2* shows the results of the 80-day-long series of Tihany; *Fig. 3* presents the spectra calculated with the 1/4, 1/2 and 3/4 parts of the 112-day-long series. The results of the observations at Obninsk are given in *Fig. 4*. For comparison the spectrum obtained from the observations with the recording gravimeter type GS—15 No. 220 of the Moscow Institute for Earth Physics "O. Yu. Schmidt" is presented in the same figure. It should be mentioned that the observations with the two instruments were conducted simultaneously in the same room. The maxima of the spectra in the diurnal frequency range are in general higher than for the frequencies of the semi-diurnal waves. The amplitudes of the residual curves have a magnitude of several tenths. For series investigated by us amplitude values of 0.20—0.30 μgal are determined on the average for diurnal and 0.05—0.25 μgal for semi-diurnal waves. Outstanding values of spectra appear either at the frequencies of the highest tidal waves or in their proximity. There is always a spectral anomaly at the frequencies of waves K_1 (P_1, S_1) and $S_2(K_2)$; at the frequencies of other waves this appears rather at random.

Anomalies of spectra calculated from residual curves which appear in the frequency range of lunisolar effects are in a significant part of events equal to error values of the harmonic analysis technique. The noise level of the presented spectra, however, is lower for non-lunisolar frequencies than in the frequency range of tidal waves. This fact seems to indicate that the recording apparatus

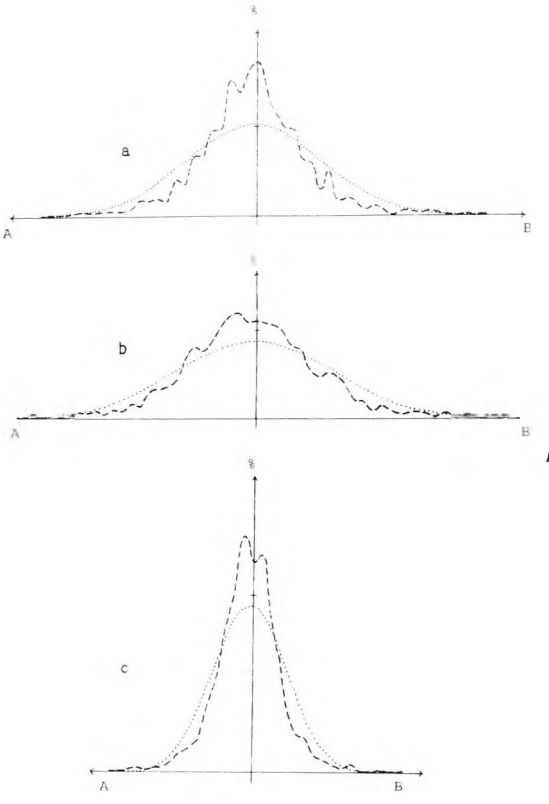

Fig. 1. Comparison of normalized distribution curves (----) calculated from drift-free residual curves of gravity earth tide observations with the Gaussian normal distribution curve (...)
a) from an 80-days' observation series at Tihany
b) from a 233-days' observation series at Obninsk
c) from a 112-days' observation series at Tihany

$$A = \frac{X_{\min} - \bar{X}}{S_x}; \quad B = \frac{X_{\max} - \bar{X}}{S_x}$$

where X_{max}, X_{min}, $\bar{X}$ are maxima, minima and average of the observed values respectively; S_x is the standard error. The interval between A and B was divided into 96 parts

1. ábra. Gravitációs földárapály megfigyelések driftmentes maradékaiból számított normalizált eloszlás görbék (– – –) és a Gauss-féle normális eloszlás görbe (···) összehasonlítása
a) Tihany 80 napos megfigyelési sorozat alapján
b) Obninsk 233 napos megfigyelési sorozat alapján
c) Tihany 112 napos megfigyelési sorozat alapján

$$A = \frac{X_{\min} - \bar{X}}{S_x}; \quad B = \frac{X_{\max} - \bar{X}}{S_x};$$

ahol X_{max}, X_{min}, $\bar{X}$ — az előforduló értékek maximuma, minimuma, illetve átlaga; S_x — standard hiba. Az A és B közötti szakaszt 96 részre bontottuk fel

Фиг. 1. Сопоставление кривых нормированного распределения (– – – –), рассчитанных по гравитационным наблюдениям за земными приливами с устранением дрейфа, и кривой нормального распределения Гаусса (. . . .):
а) Тихань, по данным серии наблюдений в течение 80-и суток;
b) Обнинск, по данным серии наблюдений в течение 233-х суток;
c) Тихань, по данным серии наблюдений в течение 112-и суток;

$$A = \frac{X_{мин} - X}{S_x}; \; B = \frac{X_{макс} - X}{S_x}$$

где $X_{макс}$, $X_{мин}$ и X – максимальная, минимальная и средняя величина встречающихся значений, а S_x – среднеквадратичное отклонение. Интервал между A и B был разделен на 96 частей.

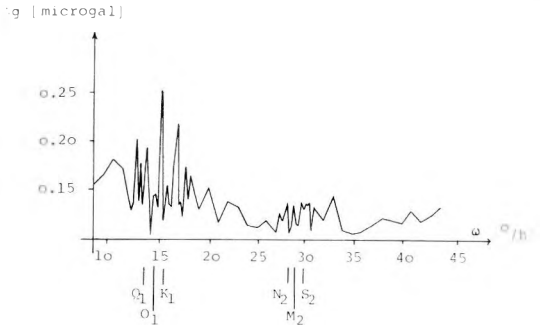

Fig. 2. Amplitude spectrum of the residual curve from the 80-days' observation series at Tihany

2. ábra. A tihanyi 80 napos megfigyelési sorozat maradék görbéjének amplitúdó spektruma

Фиг. 2. Спектр амплитуд остаточной кривой 80-суточной серии наблюдений в Тихани

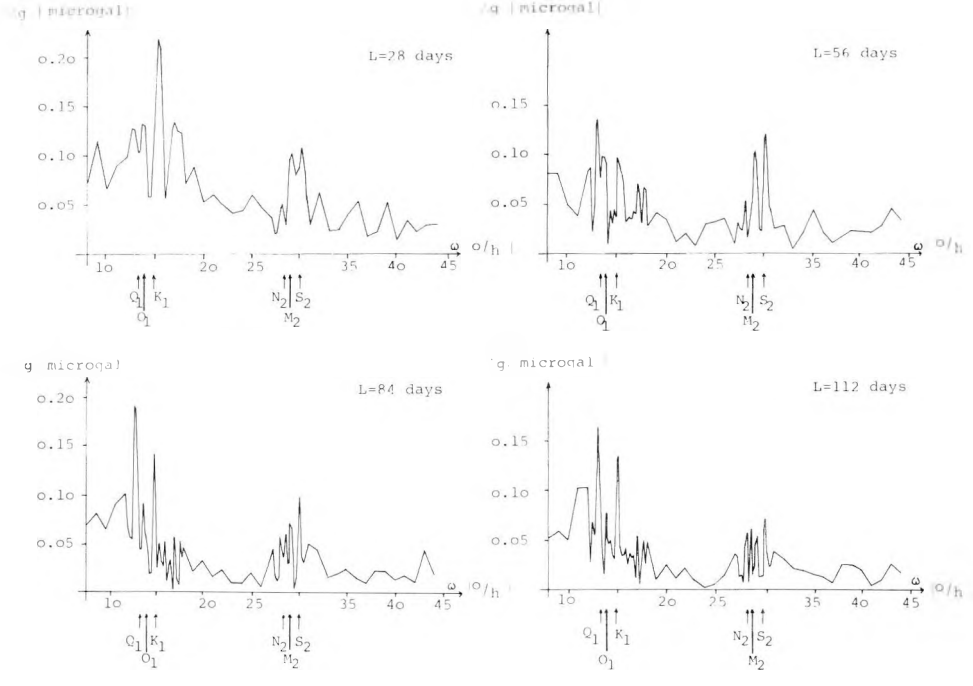

Fig. 3. Amplitude spectra of the residual curves of the 112-days' observation series at Tihany, as well as those for 1/4, 1/2 and 3/4 parts of this series

3. ábra. A tihanyi 112 napos megfigyelési sorozat, valamint 1/4, 1/2, 3/4 sorozat maradék görbéinek amplitúdó spektrumai

Фиг. 3. Спектры амплитуд остаточных кривых 112-суточной серии наблюдений в Тихани, а также серий наблюдений 1/4, 1/2 и 3/4

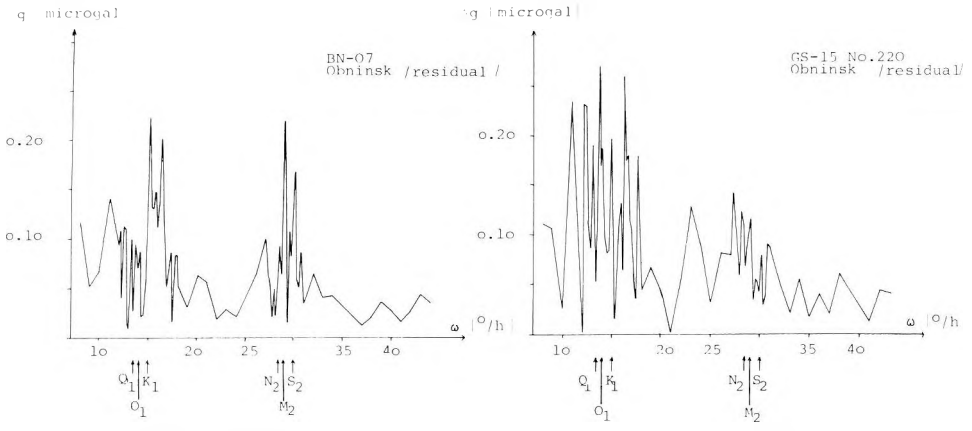

Fig. 4. Amplitude spectra calculated from residual curves of observations at Obninsk with the instruments BN—07 and GS—15 No. 220

4. ábra. A BN—07 és a GS—15 No. 220 műszerekkel Obninskben végzett megfigyelések maradék görbéiből számított amplitúdó spektrumok

Фиг. 4. Спектры амплитуд, рассчитанных по остаточным кривым наблюдений, произведенных в Обнинске приборами БН-07 и ГС-15 № 220.

permits one, in principle, to increase the accuracy of the determination of tidal parameters. Of course, the effects causing anomalies on the tidal frequencies of residual curves ought to be known. These effects are of a systematic character which—apart from the statistical investigations discussed above—follows from the fact that the residual anomalies do not decrease with increasing length of the series. Doubtless, meteorological effects also play a certain part in creating the anomalies but this relationship is not simple (the response of the instruments is not linear, it depends on frequency of temperature and air pressure variations, thus they cannot simply be excluded). It would perhaps be appropriate to put the gravity stations at a depth of 20 to 30 metres below the earth's surface. This seems to be supported by our measurements carried out at a great depth in Graz [LICHTENEGGER et al. 1982] leading to a smaller error of tidal parameters than earlier; while the drift of the instrument was 1/3 or 1/4 of the usual value.

5. Study of results of gravimeter calibrations

A factor substantially decreasing the accuracy of gravimetric earth tide observations is the inaccurate determination of record scales. In *Fig. 5* the results of instrument calibrations for the period from the end of 1974 to the middle of 1980 are summarized. Unambiguous and linear variation of the scale of records can be observed:

$$\varepsilon = 2.391\ (\mu\text{gal/mm}) + 0.048 \cdot t \left(\frac{\mu\text{gal}}{\text{mm} \cdot \text{year}} \right)$$

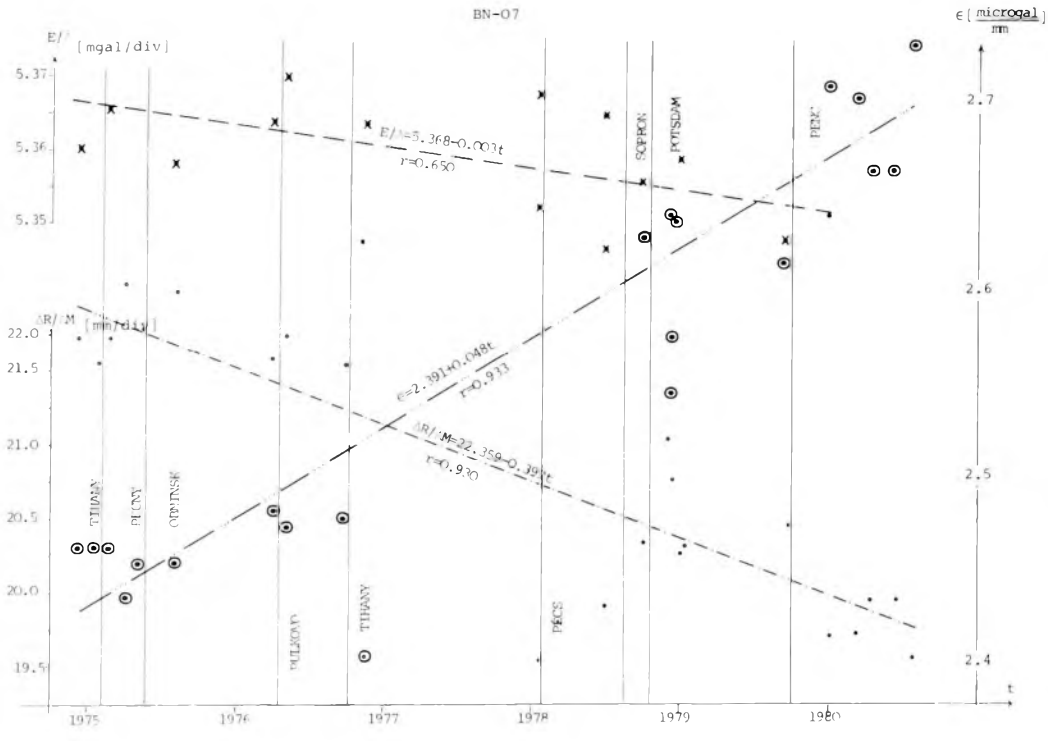

Fig. 5. Calibrations of the BN—07 instrument between 1974 and 1980

– – – determinations of the micrometer scale $\left(E/\Delta \frac{\text{mgal}}{\text{micrometer division}}\right)$;

– · – · scale of the record $\left(\frac{\Delta R}{\Delta M} \frac{\text{millimeter}}{\text{micrometer division}}\right)$;

– · · · – · · · scale of recording (in μgal/mm)

5. ábra. A BN—07 műszer hitelesítései 1974—1980 között

– – – a műszer mikrométer skálaosztásának meghatározása $\left(E/\Delta \frac{\text{mgal}}{\text{mikrométer osztás}}\right)$;

– · – · a regisztráló írószerkezetének elmozdulása

a mikrométer csavarállítás függvényében $\left(\frac{\Delta R}{\Delta M} \frac{\text{milliméter}}{\text{mikrométer osztás}}\right)$;

– · · · – · · · a regisztrálás léptéke (mikrogal/mm-ben)

Фиг. 5. Эталонировки прибора БН-07 в 1974—1980 гг.

– – – определения деления шкалы микрометра прибора $\left(E/\Delta \frac{\text{мгал}}{\text{деление шкалы микрометра}}\right)$

– · – · смещение записывающего устройства как функция наводки винта микрометра

$\left(\frac{\Delta R}{\Delta M} \frac{\text{миллиметров}}{\text{деление шкалы микрометра}}\right)$

– · · · – · · · масштаб записи (в микрогал/мм)

(correlation coefficient is 0.93). This variation can be explained by the change of the relation between the recording apparatus and the micrometer screw of the gravimeter ($\Delta R/\Delta M$). This change was not influenced by moving the apparatus from one station to another. One of the possible sources of this time-dependent variation can be the irregularities of the micrometer screw of the gravimeters. This phenomenon, however affects observation results to a limited extent only for Askania-type instruments—having an inner calibration unit—used for earth tide observations, since the time stability of such a unit is very high (see curve E/Δ in Fig. 5). The calibration of Askania-type gravimeters is discussed in detail in VOLKOV et al. [1976].

Another question is the statistical reliability of record calibrations performed within the individual measurement series themselves or of the total of observations performed at different stations. This question was studied using the ω^2 test, since within the calibrations the number of individual $\Delta R/\Delta M$ determinations is low (rarely exceeding 20), i.e. in the course of observations at individual stations the number of calibrations hardly exceeds 10. The ω^2 test offers an opportunity to check the normality of distribution for $n \sim 10$ samples [SMIRNOV and DUNIN—BARKOVSKIJ 1965], i.e. the fact that the calibrations are not burdened by systematic errors. Moreover, the determination of the parameter $\varkappa$ as recommended by MECHANIKOV [1978] was also performed. This can be determined by the formula:

$$\varkappa = \frac{\sum_{i=1}^{n} (X_i - \bar{X})^4}{n \cdot S^4},$$

where

X_i is the i-th observation,

$\bar{X}$ is the average of n observations and

$$S = \sqrt{\frac{\sum_{i=1}^{n} (X_i - \bar{X})^2}{n}}.$$

According to Mechanikov the average value of the investigated observation series approximates the true value only if $2.5 < \varkappa < 4.0$. For $\varkappa$ values strongly differing from it $\bar{X}$ is not a good estimation of the true value. Of course, one must be careful in using the latter characteristic since the selection of the interval limits of $2.5 < \varkappa < 4.0$ must be regarded as conditional only.

Table III shows the results obtained for all the calibrations performed at Graz and Potsdam. (For Potsdam the calibration values are given separately for analog and digital recording, since the observations were conducted on two channels.) It should be remarked that under the assumption of a reliability level of 0.04 the value of the ω^2 test should fall between 0.87 and 0.71. It can be seen from Table III that $\varkappa$ furnishes a satisfactory result in all three cases, though the

Station	ω^2	$\varkappa$
Potsdam (digital)	0.79	3.50
Potsdam (analog)	0.71	3.13
Graz	0.81	2.95

Table *III* Statistical evaluation of calibrations at Potsdam and Graz

III. Táblázat Potsdam és Graz állomáson végzett hitelesítések összefüggésének statisztikai értékelése

Табл. III. Статистическая оценка связи между эталонировками, произведенными на станциях Потсдам и Грац

results of analog calibration at Potsdam give a result falling on the margin of the reliability interval. *Table IV* shows the results of individual calibrations for various times without selection to illustrate the encountered values. It should be observed that on the basis of such statistical characteristics it is adequate to supervise the results of individual calibrations or eventually to omit them if both ω^2 and $\varkappa$ characteristics indicate values strongly deviate from the normal distribution.

In *Fig. 6* there are two calibration histograms (a and b) that cannot be regarded as acceptable on the basis of the ω^2 and $\varkappa$ values; in the same figure two further histograms follow that proved to be adequate. The distribution experienced in the course of calibrations leading to unfavourable results approximates the uniform distribution and the reliability of the average value is doubtful. The inner accuracy of calibrations which cannot be accepted from the statistical viewpoint, can be very good in certain instances (e.g. the inner accuracy of calibration performed on 30.10. 1978 at Penc is 0.46%, but the calibration cannot be regarded as reliable since it deviates by 2.5% from the average of all calibrations).

Summing up the foregoing it can be established on the basis of measurements carried out from 1974 to 1980 that the order of magnitude of areal variations of amplitude ratios is several tenths of a per cent and hardly exceeds the differences obtained by different instruments at a given station at the same time. Judging by the analysis of the residual curves the measurements using the BN—07 instrument (probably similarly to other instruments) is affected by systematic factors. These factors manifest themselves in a given measurement series by a given instrument. The reliability of earth tide parameters is strongly diminished if the calibrations are insufficiently reliable and statistically unfounded.

The average earth tide parameters determined on the basis of all measurements are similar to the average values obtained in other regions of the world, thus it can be established that the area investigated cannot be regarded as anomalous from the viewpoint of earth tides.

Station	ω^2	$\varkappa$
Pecný	0.92	1.66
Pecný	0.82	2.81
Pecný	0.80	2.85
Obninsk	0.80	3.15
Obninsk	0.73	3.75
Pulkovo	0.73	4.49
Pulkovo	0.73	3.54
Tihany	0.77	3.33
Tihany	0.79	1.98
Tihany	0.86	2.45
Potsdam (analog)	0.76	3.23
Potsdam (analog)	0.71	5.18
Potsdam (analog)	0.69	4.22
Potsdam (analog)	0.68	6.06
Potsdam (analog)	0.71	6.07
Potsdam (analog)	0.79	3.61
Potsdam (analog)	0.69	5.07
Potsdam (analog)	0.87	2.54
Potsdam (analog)	0.74	3.98
Potsdam (analog)	0.79	2.41
Potsdam (analog)	0.81	2.26
Potsdam (analog)	0.86	2.21
Potsdam (analog)	0.84	1.91
Potsdam (digital)	0.76	4.31
Potsdam (digital)	0.84	2.63
Potsdam (digital)	0.88	1.71
Potsdam (digital)	0.83	2.17
Penc	0.85	2.05
Penc	0.91	1.75
Penc	0.72	2.91
Penc	0.83	2.52
Penc	0.69	7.38
Graz	0.87	1.81
Graz	0.84	2.48
Graz	0.78	2.44

Table IV Statistical evaluation of individual calibrations at Pecný, Obninsk, Pulkovo, Potsdam (analog and digital), Penc, Graz

IV. Táblázat Pecný, Obninsk, Pulkovo, Potsdam (analóg és digitális), Penc, Graz állomásokon végzett egyes hitelesítések statisztikai értékelése

Табл. IV. Статистическая оценка отдельных эталонировок, произведенных на станциях Пецни, Обнинск, Пулково, Потсдам (аналоговые и цифровые), Пенц и Грац

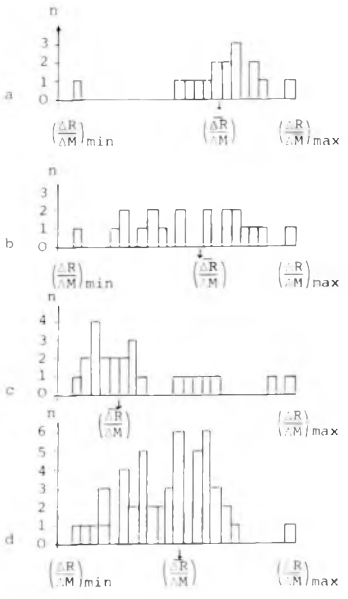

Fig. 6. Histograms of calibrations
(arrows in all figures indicate the position of the average values of $\Delta R/\Delta M$)

a. Potsdam 10. 03. 1978.
$\omega^2 = 0.683$; $\varkappa = 6.068$
b. Penc 02. 07. 1980.
$\omega^2 = 0.690$; $\varkappa = 7.377$
c. Potsdam 08. 12. 1978.
$\omega^2 = 0.797$; $\varkappa = 3.608$
d. Pecný 09. 0.4. 1975.
$\omega^2 = 0.821$; $\varkappa = 2.810$

6. ábra. Hitelesítések histogramjai
(az ábrákon nyíllal jelöltük a $\Delta R/\Delta M$ átlagértékek helyzetét)

a) Potsdam 10. 03. 1978.
$\omega^2 = 0{,}683$; $\varkappa = 6{,}068$
b) Penc 02. 07. 1980.
$\omega^2 = 0{,}690$; $\varkappa = 7{,}377$
c) Potsdam 08. 12. 1978.
$\omega^2 = 0{,}797$; $\varkappa = 3{,}608$
d) Pecný 09. 04. 1975.
$\omega^2 = 0{,}821$; $\varkappa = 2{,}810$

Фиг. 6. Гистограммы эталонировок
(положение средних значений P/M на фиг. обозначено стрелкой)

a) Потсдам 10. 03. 1978.
$\omega^2 = 0{,}683$; $\kappa = 6{,}068$
b) Пенц 02. 07. 1980.
$\omega^2 = 0{,}690$; $\kappa = 7{,}377$
c) Потсдам 08. 12. 1978.
$\omega^2 = 0{,}797$; $\kappa = 3{,}608$
d) Пецни 09. 04. 1975.
$\omega^2 = 0{,}821$; $\kappa = 2{,}810$

REFERENCES

DITTFELD, H. J., SIMON, Z., VARGA, P., VENEDIKOV, A. P., VOLKOV, V. A. 1981: Global analysis of Earth tide Observations of KAPG in Obninsk, Potsdam, Pecný, Tihany and Sofia. Study of the Earth Tides, Bulletin No. 4., Budapest.

LICHTENEGGER, H., MEURERS, B., VARGA, P. 1982: Local tide profile in Austria and Hungary. Proc. Ninth International Symp. on Earth Tides. New York (in print).

PERTSEV, B. P. 1970: The effect of ocean tides upon Earth tide observations. Communs. Observ. Roy. Belg., A9.

VENEDIKOV, A. P. 1979: Simultaneous analysis of different Earth tidal records. Merees Terrestres, Bulletin d'Informations No. 81, Bruxelles.

BOGDANOV, K. T., MAGARIK, V. A. 1969: Chislennoye reshenie zadachi o rasprostranenii prilivnyh voln v mirovom okeane (in Russian). Izvestiya AN SSSR, Fizika atmosfery i okeana, No. 12.

Volkov, V. A., Simon, Z., Varga, P., Gridnev, G. D., Dittfeld, H. J., Skalskiy, L. 1976: Metodicheskoye rukovodstvo po prilivnym nablyudeniyam s gravimetrami (in Russian). Edice VUGTK, Praha, Rada 6.

Rabinovich, S. G., 1978: Pogreshnosti izmereniy. Energiya, Leningradskoye otdeleniye

Smirnov, N. V., Dunin—Barkovskiy, N. V., 1965: Kurs teorii veroyatnostey i matematicheskoy statistiki dlya tehnicheskih prilozheniy (in Russian). Moscow, Nauka.

VARGA PÉTER

FÖLDÁRAPÁLY MEGFIGYELÉSEK A BN–07 (GS–11 No. 190) REGISZTRÁLÓ GRAVIMÉTERREL (1974—1980)

A feldolgozás 8 különböző állomáson végzett, összesen 38136 óraértéken (= 1589 nap) alapul. A földárapály görbék analízise alapján megállapítható, hogy az általunk kapott földárapály paraméterek megbízhatósága megfelel a nemzetközi szakirodalom kívánalmainak és a paraméterek jó egyezést mutatnak az elméleti földmodellek alapján számított értékekkel. Ugyanakkor ezen paraméterek területi eloszlásának vizsgálatához a jelenleginél sűrűbb állomáshálózatra van szükség. Az egy műszerrel végzett megfigyelések pontossága — műszerek csoportjával történt összehasonlítás alapján — néhány tized százalékot tesz ki, majdnem ugyanannyit, mint a BN—07 graviméterrel az egyes állomások között kapott különbség. A műszerjárás és a luniszoláris hatás kiszűrésével meghatározott maradék görbék spektrumai megmutatják, hogy a megfigyelések körülményeinek tökéletesítésével a jelenlegi műszerekkel az eddig elértnél nagyobb pontosság biztosítható. A graviméterek hitelesítésének jelenlegi nem megfelelő pontossága az a másik tényező, amely csökkenti a megfigyelési eredmények megbízhatóságát. A dolgozat ezzel kapcsolatban felhívja a figyelmet arra, hogy a hitelesítések feldolgozásának a mikrométer leolvasások statisztikai eloszlásának vizsgálatára is ki kell terjednie.

П. ВАРГА

НАБЛЮДЕНИЯ ЗА ЗЕМНЫМИ ПРИЛИВАМИ САМОЗАПИСЫВАЮЩИМ ГРАВИМЕТРОМ ТИПА БН-07 (ГС-11 № 190) в 1974–1980 гг.

В основу обработки легли наблюдения, проведенные на 8-и различных станциях в течение 38136 часов (1589 дней). Путем анализа кривых земных приливов можно установить, что надежность полученных нами параметров земных приливов соответствует требованиям, изложенным в международной специальной литературе, а сами параметры находятся в хорошем согласии со значениями, рассчитанными на базе теоретических моделей Земли. В то же время для изучения площадного распределения этих параметров требуется сеть наблюдений, более густая по сравнению с существующей. Точность наблюдений, произведенных отдельным прибором, согласно сравнению измеренных данных, полученных по группе приборов, составляет несколько десятых процента, почти столько же, как и разность значений, полученных гравиметрами БН-07 разных станций. Спектры остаточных кривых, определенных путем устранения влияния дрейфа нуля приборов и лунно-солнечных эффектов, показывают, что путем совершенствования условий наблюдений можно добиться повышения точности измерений существующими приборами. Другим фактором, снижающим надежность результатов наблюдений, является неудовлетворительная точность эталонирования гравиметров. В связи с этим в статье обращается внимание на то, что обработка данных эталонирования должна распространиться и на исследование статистического распределения отсчетов микрометра.

EÖTVÖS LORÁND GEOPHYSICAL INSTITUTE OF HUNGARY
GEOPHYSICAL TRANSACTIONS 1982
28/2 pp. 33—46

COMBINED APPLICATION OF MATHEMATICAL AND PHYSICAL MODELLING FOR POTENTIAL MAPPING

L. SZARKA*, G. SZIGETI**

The potential mapping method [PM] has had widespread application among DC exploration methods at ELGI over the last few years. To determine the PM anomalies of high resistivity basement inhomogeneities, two different approaches were used:

— conform transformation adapted at ELGI [mathematical modelling]
— analog modelling carried out at the Geodetic and Geophysical Research Institute of the Hungarian Academy of Sciences in Sopron [physical modelling].

The combined application of these methods is described and some results of applying them to actual exploration problems.

1. Introduction

During the last decade many new electromagnetic methods have been developed requiring modern techniques and difficult interpretation procedures. Meanwhile the application of DC methods has also increased as a consequence of their simplicity and cheapness. In view of this, further development of DC interpretation methods became necessary.

Since 1980 the methodological and interpretation problems connected with high resistivity basement inhomogeneities of some DC exploration methods have been solved cooperatively by ELGI and the Geodetic and Geophysical Research Institute of the Hungarian Academy of Sciences (MTA GGKI). This cooperation aims to determine the distorting effects of two- and three-dimensional basement structures on the electric field using both mathematical and physical modelling.

2. Theory of the potential mapping method

Potential mapping [PM] means the measuring of the quasi-stationary electric field on the surface between two distant electrodes A and B. *Figure 1* shows a typical measuring arrangement of the PM method used in practice.

For high resistivity basement structures the two layered half space with a ϱ_∞ resistivity bottom is the basic model. The measured field strength anomalies on the surface are caused by the horizontal inhomogeneities of the basement surface.

The measured values of the electric field strengths are transformed as follows:

* Geodetic and Geophysical Research Institute of the Hungarian Academy of Sciences, Sopron
** Eötvös Loránd Geophysical Institute of Hungary, Budapest
Paper presented at the 26th Geophysical Symposium, Leipzig, 22—25 September, 1981.

$$S_m = -\frac{E^{\text{basic model}}}{E^{\text{measured}}}$$

where E represents the field strength. The S_m profile (or S_m map) will be similar to the surface of the high resistivity basement. This S_m distribution is called a PM anomaly.

In model calculation and model measurements M_1 means the depth of the basement far from the inhomogeneities, M_2 the depth of the basement inhomogeneities. The anisotropy coefficient is assumed to be 1.

In this paper the PM anomalies of faults, horsts and trenches will be determined. In geology these basement inhomogeneities are called "structural elements", but for simplicity we shall call them "structures".

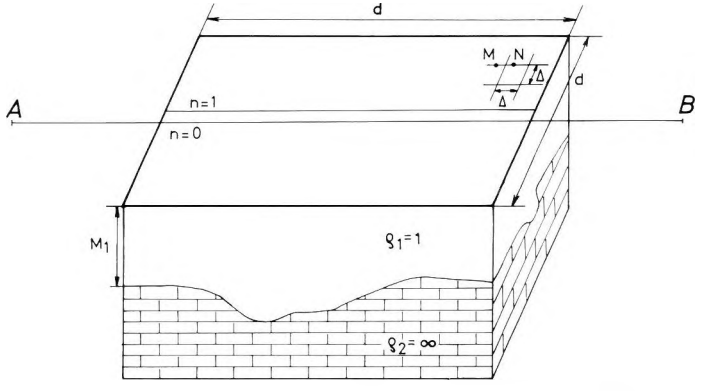

Fig. 1. Typical measuring arrangement of potential mapping method
M_1—average depth of basement; A and B—current electrodes, usually AB ≈8—10M_1; M and N—measuring electrodes; Δ—distance between measuring points; d—length of side of survey area, usually $d \approx 4—5M_1$; n—serial number of profile ($n=0$: base line, $n = 1, 2, \ldots$: side profiles)

1. ábra. Potenciáltérképezés tipikus mérési elrendezése
M_1 — az aljzat átlagmélysége; A és B — áramelektródák, szokásosan AB ≈8—10M_1; M és N — mérőelektródák; Δ — mérési ponttávolság; d — mérési terület oldalmérete, $d \approx 4—5M_1$; n — szelvény sorszáma ($n=0$: bázisszelvény, $n=1, \ldots$ oldalszelvények)

Рис. 1. Типичное измерительное расположение в методе потенциального картировании (*PM*)
M_1 — средняя глубина основа высокого сопротивления; A, B — электроды тока, обыкновенно $AB \approx 8-10M_1$; M, N - измерительные электроды; Δ — дистанция между точками измерений; d — длина сотороны измерительной территории, обыкновенно $d \approx 4-5M_1$; n — номер профиля измерений ($n = 0$: основной профиль, $n = 1, 2, \ldots$: боковые профили)

3. Short description of the modelling methods

There are two methods of determining the disturbing effect of some high resistivity structures placed in a two-layered half space in the electric field:

— a mathematical method, i.e. the so-called conform transformation (used at ELGI),
— an analog geoelectric modelling technique (developed in the electromagnetic modelling laboratory of MTA GGKI).

3.1. Conform transformation

The electric field distortion of 2D high resistivity basement structures is determined with infinitely long line sources.

A detailed description of this method can be found in [SZIGETI 1980]. The basic idea is as follows.

There is a close connection between the conform transformation and the Laplace equation, i.e. the Laplace equation is invariant to the conform transformation. The complex potential function f of a stripe-like range $-1 \leqq \mathrm{Im}\, z \leqq 0$ with a source at z_0 can easily be determined:

$$f = \ln(\mathrm{ch}\, z - \mathrm{ch}\, z_0).$$

If for a given range Ω_w the $z = g(w)$ function (which transforms from Ω_w into the stripe $-1 \leqq \mathrm{Im}\, z \leqq 0$) is produced (*Fig. 2*), and the source is in w_0, the $p(w)$ complex potential function of the range Ω_w can be expressed as follows:

$$p(w) = f[g(w)] = \ln[\mathrm{ch}\,[g(w)] - \mathrm{ch}\,[g(w_0)]].$$

According to Rieman's theorem concerning the conform transformations, such a function $g(w)$ always exists. This $g(w)$ has also to fulfil the conditions

$$g(\pm\infty) = \pm\infty, \qquad g'(\infty) = 1.$$

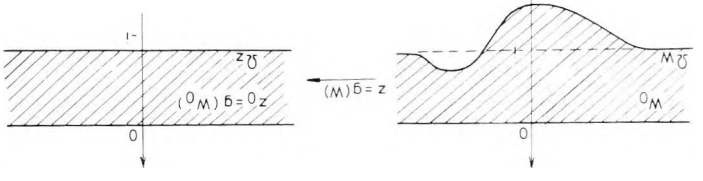

Fig. 2. Derivation of conform transforming function $g(w)$
Ω_w—stripe-like range to be transformed; w_0—position of source; Ω_z—two layered basic model (stripe); z_0—position of source in basic model

2. ábra. A konform leképezés $g(w)$ függvényeinek származtatása
Ω_w — leképezendő sávszerű tartomány; w_0 — forrás helye; Ω_z — kétréteges alapmodell, azaz sáv; z_0 — forrás helye az alapmodellben

Рис. 2. Происхождение функции комплексной трансформации
Ω_w — изображаемая область похожа на полосу; w_0 — позиция источника; Ω_z — двухслойный основной модель (полоса); z_0 — позиция источника в основном модеде

If, therefore, the transforming function $g(w)$ and the complex potential $p(w)$ are known, each field characteristic, among others the surface electric field strength, can be determined.

Until now the conform transforming functions $g(w)$ for structures described in *Fig. 3* have been designed.

In this paper only the geological correspondence of the models and the solution method of $g(w)$ are dealt with. Some formulae will be presented in the following section. The structures *a* and *b* in Fig. 3 are models of horsts; *c* and *d* are faults; *e* and *f* are models of depressions.

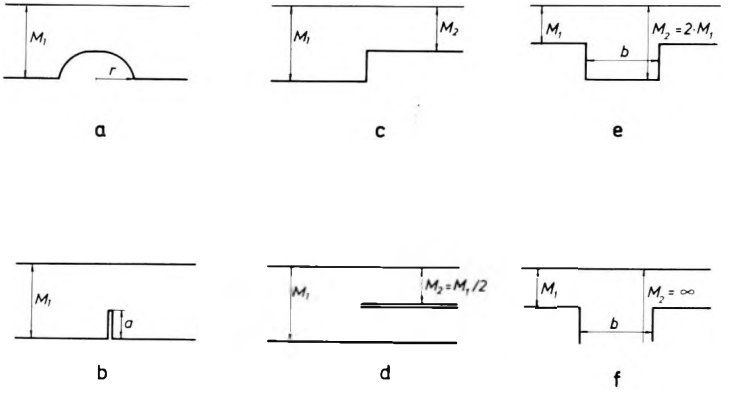

Fig. 3. Structures studied by conform transformation
M_1—depth to basement; *r*, *a*, *b*—for fixed M_1 these variables can be changed without restriction; M_2—fixed values in the models

3. ábra. A konform leképezések módszerével tanulmányozott kétdimenziós szerkezetek
M_1 — torzítatlan aljazmélység; *r*, *a*, *b* — az M_1-hez képest tetszőlegesen változtatható geometriai paraméterek; M_2 — a modellekben rögzített értékek

Рис. 3. Двухмерные структуры изученные методом комплексной трансформации
M_1 — глубина основа высокого сопротивления; *r*, *a*, *b* — геометрические параметры, по сравнению M_1 они могут принять любие величины; M_2 — фиксированные величины в моделях

Model *a*, is a modified version of the semicylinder described in [Szigeti 1980]. The surface unevenness could be removed by a small distortion of the form of the structure. There is a close connection between the height and the radius of the modified semicylinder.

Models *c* and *f* represent geologically interesting structures, for which the application of the Schwarz—Christoffel formula does not meet difficulties in determining its constants. In case *f*, (infinitely deep trench) the symmetry principle of the theory of complex functions was also exploited [Lavrentiev, Sabin 1959].

In cases *b* (an infinitely thin horst) and *d* (a high resistivity half-plane in the layer) the function $g(w)$ can be obtained by a combination of elemental functions.

The anomaly of model *e* (where the depth of the trench equals the thickness of the layer) was obtained in the same way as in case *d*, but here some physical considerations were also taken into account.

3.2. DC geoelectric analog modelling

Analog modelling of the DC exploration methods has been developed in the modelling laboratory of MTA GGKI *(Fig. 4)* [ÁDÁM et al. 1981, SZARKA 1980].

The models of basement inhomogeneities are built on the bottom of a 3×4 m plastic modelling tank containing sodium chloride solution. The measurements are carried out on the surface of the electrolyte. The modelling frequency of 500 Hz is low enough to produce a quasi-stationary field in the medium with a resistivity of about 0.1 Ωm. The potential differences on the measuring dipole of the rolling bridges are punched automatically on tape.

With analog modelling the electric field distortion effects of both 2D and 3D basement inhomogeneities can be examined. All geometric modelling parameters should be exactly proportional to the real parameters on the field.

Not only perfect insulators, but also very well conducting structures can be modelled with this equipment.

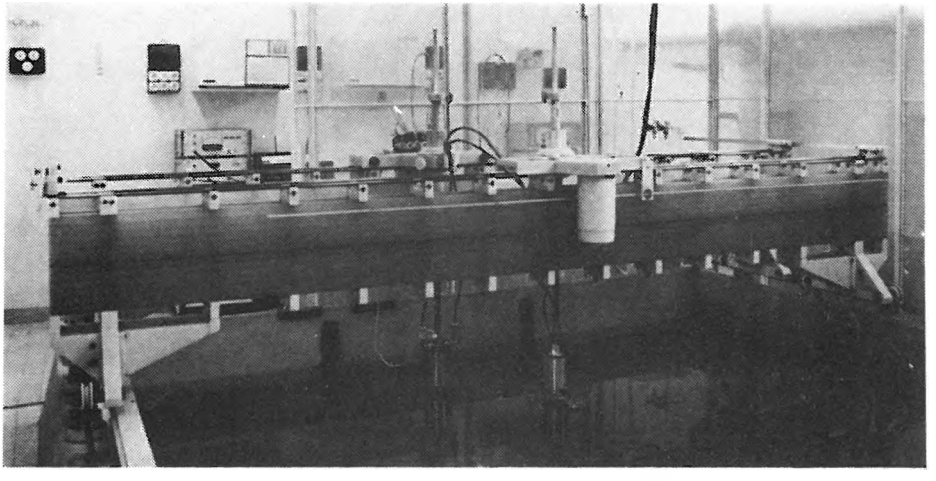

Fig. 4. Electromagnetic modelling laboratory at the Geodetic and Geophysical Research Institute of the Hungarian Academy of Sciences, Sopron

4. ábra. Az MTA Geodéziai és Geofizikai Kutató Intézetében működő elektromágneses modellező berendezés

Рис. 4. Електромагнитная моделизирующая лаборатория в Исследовательском Институте Геодезии и Геофизики АН ВНР

3.3. Potentialities of conform transformation and analog modelling in exploring high resistivity basement inhomogeneities

The conform transformation method can examine only strictly 2D cases, where not only the structure but also the source is two dimensional, and the source line is parallel with the strike of the structure. In physical modelling there is no such limitation.

Both methods can deal with the case of a perfect insulating basement.

The most practical model forms in analog modelling are rectangular prisms. From among prism-like models only the faults (model *c*, Fig. 3) and one special case of trenches (model *e*, Fig. 3) can be examined by conform transformation. On the other hand a study of the mathematically limiting cases of these prism-like structures does not meet any difficulties using conform transformation, while naturally they cannot be built in the model tank.

An advantage of conform transformation over other mathematical methods is that the anomaly curves can be calculated analytically, and the geometric parameters as well as the position of the source can be varied very simply and without any restriction.

The advantage of analog modelling is that the character of the model structures and that of the sources are more similar to the field conditions. On the other hand the model measurements need more time and the results contain measuring errors.

In section 4.1 it will be shown that above 2D structures the conform transformation anomalies agree with analog modelling anomalies. This means that combined application of these two methods enables any problem of 2D and 3D high resistivity basement structures to be solved.

4. Examples of combined applications of mathematical and physical modelling

4.1. Agreement of PM anomalies using line and point sources above 2D basement structures

As a first step, the S_m profiles above a steplike fault obtained by these two methods were compared, to decide if they can be used jointly.

To calculate the S_m curve the inverse of the transforming function $g(w)$ can be written as follows (in somewhat different form see Fig. 30 of table 7.9.2. in [KORN and KORN 1961]):

$$w = g^{-1}(z) = \frac{M_2}{\pi} \ln \left(\frac{\sqrt{M_1} z + \sqrt{M_2}}{\sqrt{M_1} z - \sqrt{M_2}} \right) +$$

$$+ \frac{M_1}{\pi} \ln \left(\frac{\sqrt{M_1} - \sqrt{M_2} z}{\sqrt{M_1} + \sqrt{M_2} z} \right)$$

In *Fig. 5* the continuous line represents the anomaly curve obtained by mathematical modelling and the crosses demonstrate the results of the physical modelling along a profile connecting the current electrodes A and B. The agreement means that the conform transformation gives a physically realistic S_m anomaly for real field conditions. (A similar agreement was obtained in the case of other 2D structures.)

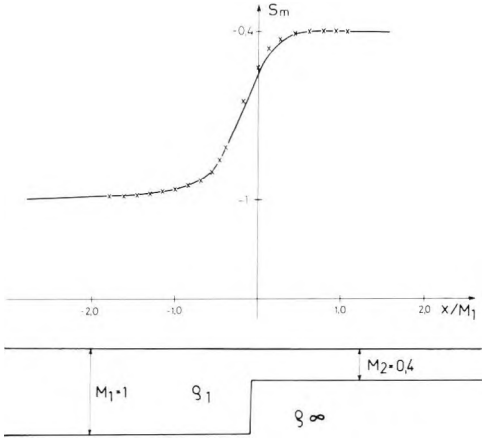

Fig. 5. PM anomalies obtained by mathematical and physical modelling above a 2D fault in the high resistivity basement ——— result of mathematical modelling; *x*—results of physical modelling

5. ábra. Matematikai és fizikai modellezéssel nyert PM-anomália, nagy ellenállású medencealjzatban lévő vető fölött ——— matematikai modellezés eredménye; *x* — fizikai modellezés eredménye

Рис. 5. PM-аномалия полученная математическим и физическим моделированиями над двухмерным сбросом в основе высокого сопротивления ——— математическое моделирование; *x* — физическое моделирование

Analog modelling showed that above 2D structures the PM anomaly in the base line agrees with the PM anomalies in all side-profiles running parallel to the AB line.

Another practical significance of Fig. 5 is the following. The horizontal position of the fault is not correctly at the abscissa of the inflexion point. The exact position of the fault as a function of the faulting height and the faulting angle has been determined by analog modelling.

As physical modelling had confirmed the reliability of the conform transformation, a "faultcatalogue" was compiled at ELGI exploiting the flexibility of this computer method against variations of the geometric parameters. This set of master curves contains S_m curves of step-like faults for optional parameters [SIMON et al. 1981].

It must be mentioned that if the structure is close to one of the current electrodes, the S_m profiles obtained by these two methods are not identical any more, only their characters are similar. The deviation is due to the fact that the requirement of the structure being two-dimensional was no longer fulfilled for the mathematical method.

4.2. Effect of faulting angle on PM anomaly

In order to determine the effect of variation in the faulting angle model measurements were made above faults with different faulting angles: $\alpha = 15°$, 45°,

90°, 135° and 165°. From *Fig. 6* it can be seen that it is impossible to find any difference between PM anomalies of the steplike faults ($\alpha = 90°$) and that of the overthrust ($\alpha > 90°$). The parallel displacement of the curves is derived only from the different positions of the structures.

The complete agreement of the S_m curves calculated for models *c* and *d* in Fig. 3 is in accordance with the result of analog modelling.

Model *d* in Fig. 3 can be interpreted as a mathematical limiting case of the overthrusts in the physical experiment.

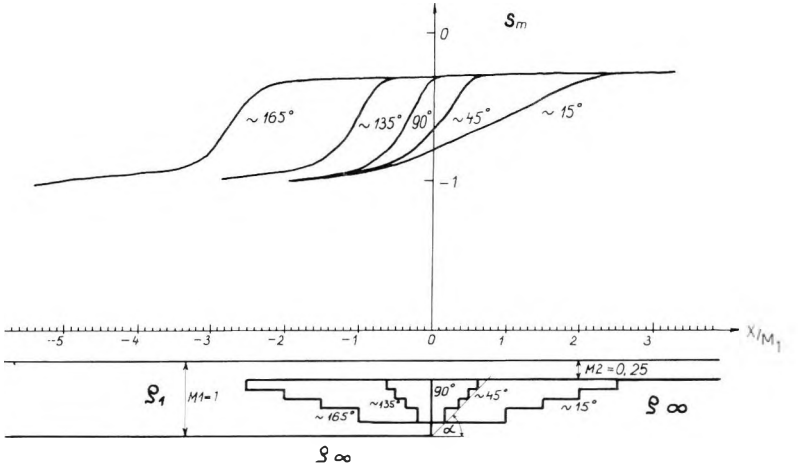

Fig. 6. Effect of faulting angle on PM anomaly
α—faulting angle

6. ábra. Az elvetési szög hatása a vető PM-anomáliájára
α — a vető dőlésszöge

Рис. 6. Влияние угла сброса на *PM*-аномалию
α – угол сброса

4.3. PM anomalies of 2D horsts and trenches

We examined how the PM anomaly follows the variation of the width of two dimensional structures.

As can be seen from Fig. 5, the asymptotes of the PM anomaly curve correspond to the real S_m horizontal conductances on the downthrown and on the elevated sides of the fault.

It is important to know how wide the high resistivity horst and trench should be to obtain an S_m value equal to the real value of the horizontal electric conductance above the structure.

Figure 7 shows a measured series above several high resistivity horsts.

Figure 8 summarizes the PM anomaly extremes of all prism-like 2D high resistivity structures as a function of the relative width b/M_1. The curve parameter is M_2/M_1.

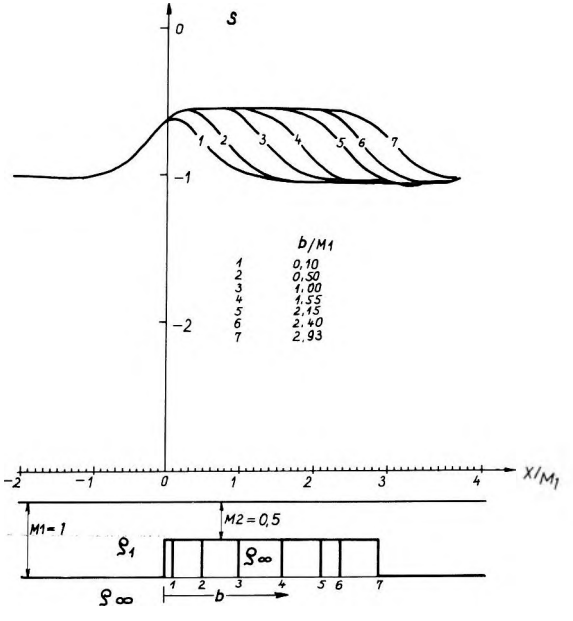

Fig. 7. Effect of variation in width of 2D horsts on the PM anomaly

7. ábra. 2D sasbércek szélességváltozásának hatása a PM-anomáliára

Рис. 7. Влияние изменения ширины двухмерных горстов на *PM*-аномалию

PM anomalies of horsts and trenches were partly physically modelled, partly calculated by conform transformation. Extremes of anomalies for models having finite parameters were determined by analog modelling. For some mathematically limiting cases, which cannot be built in the model tank (Fig. 3, models *b* and *f*), and for a trench of depth $M_2 = 2M_1$ (Fig. 3, model *e*) some simpler formulae can be derived if the transforming function $g(w)$ is known.

Let $S_m(0)$ mean the extreme of an S_m profile, having its extreme at $x = 0$. For model *b*:

$$S_m(0) = -\cos\left(\frac{\pi a}{2}\right)$$

For model *e*:

$$S_m(0) = -\frac{2\left(e^{\pi\frac{b}{2}}+1\right)}{e^{\pi\frac{b}{4}}+1}$$

For model f:

$$S_m(0) = -\sqrt{\left(\frac{b}{2}\right)^2 + 1}\,.$$

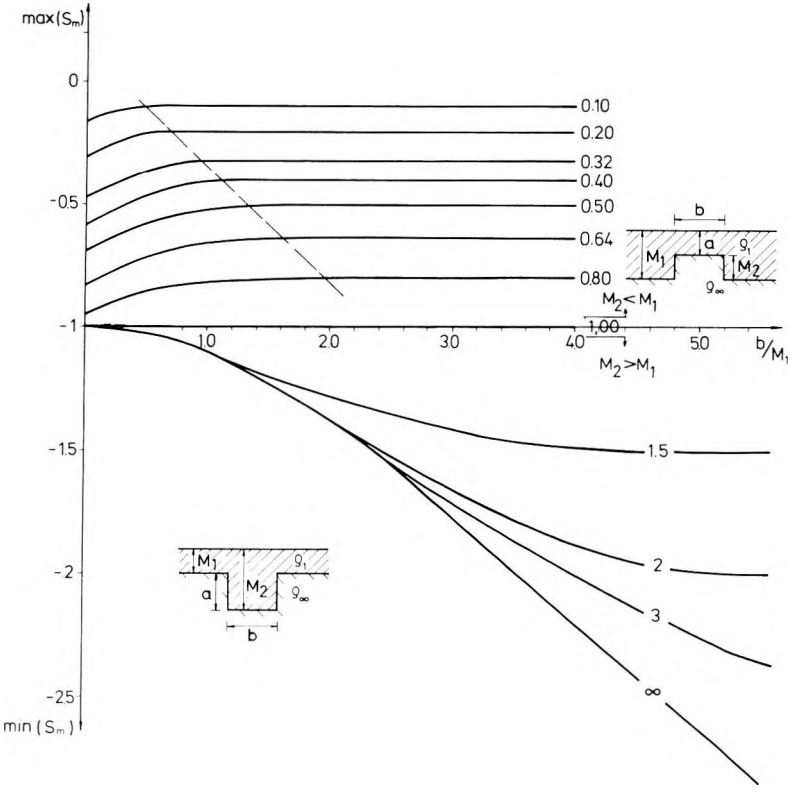

Fig. 8. Extreme values of PM anomalies for 2D horsts and trenches versus width of the structure. The curve parameter is M_2/M_1

8. ábra. 2D sasbércek és árkok anomália-szélsőértékeinek alakulása a szerkezet szélességének függvényében. A görbeparaméter M_2/M_1

Рис. 8. Экстремальные значения *PM*-аномалии двухмерных горстов и ровов в функции ширины структуры. Параметр кривы: M_2/M_1

On the basis of Fig. 8 for the case of horsts ($M_2/M_1 < 1$) the following statements can be made:

— with wider horsts ($b/M_1 > 1$), the extreme values $S_m(0) = \max(S_m)$ are linear functions of M_2/M_1.

— with narrower horsts ($b/M_1 < 1$) the linear depth-calculation method cannot be applied. The limit of the applicability of the linear depth-calculation is denoted roughly by the dashed line in Fig. 8.
— using the PM method, a narrow horst and a wider horst can be in equivalence. *Figure 9* shows a mathematical example for this where the S_m profiles of the rounded and those of the needle-like structures cannot be distinguished.

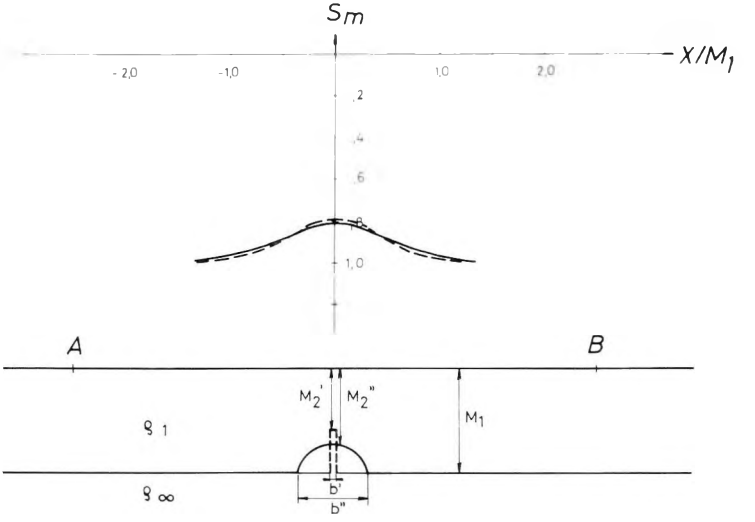

Fig. 9. Equivalent horsts in the PM method. For needle-like structure $b' \approx 0$, $M' = 0.59$; for rounded structure $b'' = 0.66$, $M_2'' = 0.66$

9. ábra. Ekvivalens hatású nagy ellenállású medencealjzat-kiemelkedések
A tűszerű kiemelkedésnél $b' \approx 0$, $M_2' = 0{,}59$, a lekerekített kiemelkedésnél $b'' = 0{,}66$, $M_2'' = 0{,}66$

Рис. 9. Эквивалентные горсты в методе *РМ*. В случае структуры форма «игли» $b' \approx 0$, $M_2' = 0{,}59$, в случае округленной структуры $b'' = 0{,}66$; $M_2'' = 0{,}66$.

Concerning the trenches Fig. 8 shows the following conclusions:
— using the PM method very narrow trenches ($b/M_1 < 0.5$) cannot be detected at all.
— in the range $0.5 < b/M_1 < 1$—2 (the exact limiting values depend also on M_2/M_1) there is no difference between the PM anomalies of trenches having finite and infinite depth (e.g. a difference between curves having the parameters $M_2/M_1 = 2$ and $M_2/M_1 \to \infty$ appears only if $b/M_1 > > 2.2$).
— for $b/M_1 > 1$—2, the bottom of the trenches can be detected, but the anomaly is less than it should be according to the real horizontal conductance above the trench.
— linear depth-calculation can be applied only with very wide trenches (e.g. if $M_2/M_1 = 1.5$, $b/M_1 > 4$).

Summarizing the conclusions of Fig. 8, the PM anomalies of 2D horsts and trenches differ from each other. Contrary to trenches, already narrow horsts have significant anomalies. The linear depth-calculation is more often adaptable for horsts than for trenches.

4.4. PM anomalies of 3D horsts

In the model tank the width (b) of the horst was fixed and the length (L) of the structure was varied in the range $0.1 < L/M_1 < 15$. The conclusions of these measurements are shown in *Fig. 10.* The values β_n mean the quotient of the

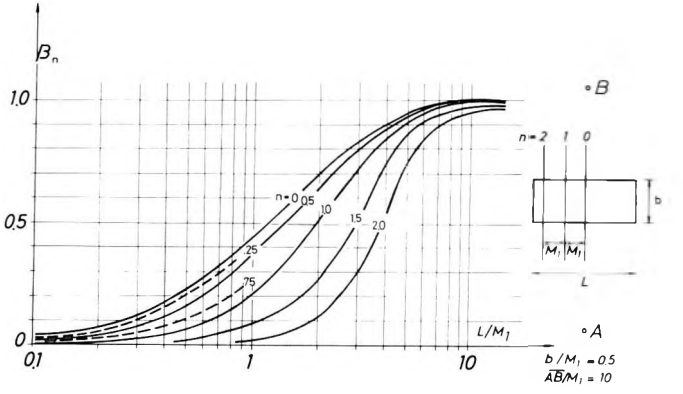

Fig. 10. Comparison of PM anomaly maxima above 3D horsts with anomaly maxima above 2D structures
L—length of 3D structure; n—number of profiles. Distance between profiles is M_1

$\beta_n = \dfrac{\max S_m(L, n)}{\max S_m(\infty, 0)}$, where the numerator means the S_m extreme above the 3D structure of length L at profile n; the denominator means the S_m extreme above a 2D structure having the same cross-section

10. ábra. Háromdimenziós PM anomália-maximumok összehasonlítása a 2D szerkezetek fölötti értékekkel
L — a 3D kiemelkedés hossza; n — a szelvény sorszáma. A szelvények távolsága M_1.
$\beta_n = \dfrac{\max S_m(L, n)}{\max S_m(\infty, 0)}$, ahol a számláló az L hosszúságú modell fölött áthaladó n jelű szelvényen kapott szélsőérték. A nevező az ugyanolyan keresztmetszetű 2D sasbérc fölötti szélsőértéket jelzi

Рис. 10. Сравнение максимальных значений *PM*-аномалий над трёхмерными горстами и максимальных значений над двухмерными структурами
L — длина трёхмерной структуры; n — номер профиля. Дистанция между профилями M_1
$\beta_n = \dfrac{\max S_m(L, n)}{\max S_m(\infty, 0)}$, где числитель значит экстемальное значение S_m над трёхмерной структурой в профиле n, знаменатель значит экстремальное значение S_m над двухмерной структурой имеющей точно такого поперечного сечения

max (S_m) above the 3D horst in different profiles to the maxima of S_m above the 2D limiting case; $n=0$ means the base-line. The curve $n=0$ shows that, for example, the PM anomaly maxima of a 3D horst having $L=3M_1$ is about 83% of the anomaly of the corresponding 2D structure, and a horst situated about the normal bisector of the AB layout can be regarded as a 2D one only if $L/M_1 > 10$. (A similar critical value has been obtained also for trenches.)

Thus it is possible to decide by analog modelling if for a given 3D field exploration problem 2D interpretation methods could be applied or not.

5. Conclusions

The properties and the potentials of conform transformation are different from those of analog modelling. Therefore with combined application the sphere of solvable problems becomes greater.

Having proved that PM anomalies of 2D structures obtained using a line and a point source agree, a very wide range of 2D problems can be solved by conform transformation.

An examination of models which can be solved by both methods serves as a control.

Physically non-examinable but geologically interesting mathematical limiting cases can also be solved easily by conform transformation. The limits of application of 2D mathematical methods can be sought by analog modelling.

In analog modelling we currently study PM anomalies of 3D basement inhomogeneities and deal with the elaboration of measuring possibilities of multilayered problems. In the meantime, transform functions for more and more complicated 2D structures are being developed.

Conform transformation cannot be used to solve 3D problems. Nowadays this problem can be solved only by analog modelling but this method cannot disregard the knowledge of the exact mathematical solutions obtained for 2D structures by conform transformation.

Our combined methods are suitable for a detailed examination of other DC exploration methods too.

REFERENCES

ÁDÁM, A., PONGRÁCZ, J., SZARKA, L., NAGY, Z., ZIMÁNYI, I., KARDEVÁN, P., SZABADVÁRY, L., KORMOS, K., RÉGENI, P. 1981: Analog model for studying geoelectric methods at the GGRI of the Hung. Ac. Sci. Acta Geod. Geoph. Mont. Hung. **16,** pp. 359—380.

KORN, G. A., KORN, T. M. 1961: Mathematical Handbook for Scientists and Engineers. McGraw-Hill Book Company, New York.

LAVRENTIEV, M. A., SABIN, B. V. 1959: Methods in the Theory of Complex Functions (in Russian), State Publ. House of Phys. Mat. Lit., Moscow.

SIMON, A., SZABADVÁRY, L., SZARKA, L., SZIGETI, G. 1981: Direct current mathematical and physical modelling. Annual Report of ELGI for 1980, pp. 165—167.

SZARKA, L. 1980: Analog modelling of the potential mapping method (in Hungarian). Magyar Geofizika, **21,** 5, pp. 193—200.

SZIGETI, G. 1980: Application of the conform transformation method to determine the electric field distribution above a high resistivity semicylinder using line source field generation (in Hungarian). Magyar Geofizika, **21,** 4, pp. 121—133.

SZARKA LÁSZLÓ, SZIGETI GÁBOR

MATEMATIKAI ÉS FIZIKAI MODELLEZÉS EGYÜTTES ALKALMAZÁSA A POTENCIÁLTÉRKÉPEZÉS FELADATAINAK MEGOLDÁSÁBAN

Az egyenáramú módszerekkel vizsgálható feladatok megoldásában az ELGI az egyszerű és gyors potenciáltérképezést (PM) néhány éve kiterjedten alkalmazza. A nagy ellenállású medencealjzat-inhomogenitások PM-anomáliáinak meghatározására két módszert használtunk:

— az ELGI-ben adaptált konform leképezések módszerét (matematikai modellezés),
— Sopronban, az MTA GGKI-ben végzett geoelektromos analóg modellezést (fizikai modellezés).

A tanulmány a két módszer együttes alkalmazásának lehetőségeit körvonalazza, valamint bemutat néhányat a gyakorlatban is felhasznált közös eredmények közül.

Л. САРКА, Г. СИГЕТИ

КООРДИНИРОВАННОЕ МАТЕМАТИЧЕСКОЕ И ФИЗИЧЕСКОЕ МОДЕЛИРОВАНИЕ В МЕТОДЕ ПОТЕНЦИАЛЬНОГО КАРТИРОВАНИЯ

Метод потенциального картирования (PM) играет значительную роль среди других методов постоянного тока применённых в ELGI. Для решения PM-аномалий структур основа высокого сопротивления исследования проводились в двух направлениях:

– математическое исследование проведенное в ELGI по так называемому методу комплексной трансформации (математическое моделирование),
– аналоговое моделирование проведенное в Исследовательском Институте Геодезии и Геофизики АН ВНР (физическое моделирование).

В этой стати написаны возможности координированного применения этих методов и показаны некоторых результатов прикладных в практике.

EÖTVÖS LORÁND GEOPHYSICAL INSTITUTE OF HUNGARY
GEOPHYSICAL TRANSACTIONS 1982
28/2 pp. 47—56

INTERPRETATION OF IN-MINE GEOELECTRIC SOUNDINGS BY MEANS OF KERNEL FUNCTIONS

Á. GYULAI*

The principal aim of geoelectric soundings performed in drifts is to provide thickness data of seams and protective layers for guiding mining activity. Sounding curves can be interpreted either by comparing the measured resistivity curves with a set of master curves, or by the use of kernel functions. The paper presents a method of interpretation and programs written for the TI—59 desk-top computer.

1. Introduction

In-mine vertical electric soundings are usually interpreted by comparison with a theoretical chart of specific resistivity curves. In coal mines, for example, the method is used for the determination of the thickness of the protective layer—a task that even in the simplest case implies a four-layer geophysical model since, even for high specific resistivity coal beds, the electric field has to be taken into account for sufficiently large distances. In the majority of cases the curves should be computed for four or even more layers [CSÓKÁS 1980], a rather complicated task for desk-top computers. It seems reasonable to adopt the kernel function method, widely used in the interpretation of surface VES measurements [KOEFOED 1979], that transforms the specific resistivity curve into a kernel-function curve and yields an easier means for the computation of the layer parameters.

2. Transformation of the points of the specific resistivity curve into a kernel function $R(m)$

As is well known [VAN NOSTRAND and COOK 1966], if we introduce current into some layer of specific resistivity ϱ_j of an n-layered medium, the potential in layer i will be given by

$$U_i = \frac{\varrho_j^I}{4\pi}\left[\frac{1}{R} + \int_0^\infty [A_i e^{-mz} + B_i e^{mz}] J_0(mr)dm\right] \tag{1}$$

* Geophysics Department, University of Heavy Industry, Miskolc, Hungary
Manuscript received (revised form): 5. 5. 1982.

In particular, if the source is placed on any of the boundaries of the second layer the potential at the same boundary is:

$$U_2 = \frac{\varrho_2' I}{4\pi} \int_0^\infty R_2'(m) J_0(mr) dm, \tag{2}$$

where

$$R_2(m) = A_2(m) + B_2(m) + 1 \tag{3}$$

and

$$R_2(m) = R_2'(m) \cdot \varrho_2. \tag{4}$$

From Eq. (2) the apparent specific resistivity for a four-electrode Schlumberger arrangement can be expressed as:

$$\varrho_a = r^2 \int_0^\infty R_2(m) m J_1(mr) dm, \tag{5}$$

where $r = AB/2$.

Equation (5) yields, after some rearrangements and by application of the inverse Hankel transform:

$$R_{2\text{top}}(m) = R_T(m) = \varrho_{12} + \int_0^\infty \frac{\Delta\varrho}{r} J_1(rm)\, dr, \tag{6}$$

that corresponds to a sounding carried out at the boundary between the first and second layers ("top" sounding). In Eq.(6), $\varrho_{12} = \dfrac{\varrho_1 \varrho_2}{\varrho_1 + \varrho_2}$ is the resultant specific resistivity obtained from the half-space geometry of the first and second layers, connected in parallel; $\Delta\varrho$ denotes the deviations of the top sounding curves from this value, that is

$$\Delta\varrho(r) = \varrho_{a(\text{top})} - \varrho_{12}. \tag{7}$$

For the "floor" sounding at the boundary between the second and third layer the same equations (6, 7) remain valid with ϱ_{12} substituted by ϱ_{23}.

3. The $R'_T(m)$ function for the top sounding

The value $R'_2(m)=R'_T(m)$ can be determined from the linear system of equations, describing the physical boundary conditions and containing $A_2(m)$ and $B_2(m)$ as unknowns [GYULAI 1979].

For a four-layered model, if the floor consists of two layers

$$R'_T(m)=\frac{(1+k_{12})[1+k_{23}k_{34}e^{-2mb'}-k_{23}e^{-2mb}-k_{34}e^{-2m(b+b')}]}{1+k_{23}k_{34}e^{-2mb'}+k_{12}k_{23}e^{-2mb}+k_{12}k_{34}e^{-2m(b+b')}} \tag{8}$$

(see *Fig. 1*). From the formula for $R'_T(m)$ we can express the thickness b of the coal bed, and the thickness b' and specific resistivity ϱ_3 of the protective layer as follows:

$$b=\frac{\ln\dfrac{[1+k_{12}-R'_T(m)][1+k_{23}k_{34}e^{-2mb'}]}{[1+k_{12}+k_{12}R'_T(m)][k_{23}+k_{34}e^{-2mb'}]}}{-2m}, \tag{9}$$

$$b'=\frac{[1+k_{12}-R'_T(m)]-[1+k_{12}+k_{12}R'_T(m)]k_{23}e^{-2mb}}{-k_{23}k_{34}[1+k_{12}-R'_T(m)]+[1+k_{12}+k_{12}R'_T(m)]k_{34}e^{-2mb}}}{-2m} \tag{10}$$

$$\varrho_3^2+[B(A\varrho_2+\varrho_4)]\varrho_3+A\varrho_2\varrho_4=0, \tag{11}$$

where

$$A=\frac{\dfrac{[1+k_{12}-R'_T(m)]e^{2mb}}{1+k_{12}+k_{12}R'_T(m)}-1}{\dfrac{[1+k_{12}-R'_T(m)]e^{2mb}}{1+k_{12}+k_{12}R'_T(m)}+1} \tag{12}$$

and

$$B=\frac{e^{-2mb'}+1}{e^{-2mb'}-1}. \tag{13}$$

4. The $R'_F(m)$ function for the floor sounding

For a four-layered model (*Fig. 1*), $R'_2(m)=R'_F(m)$ can be obtained from the kernel functions $A_2(m)$ and $B_2(m)$ [GYULAI 1979].

$$R'_F(m)=\frac{(1-k_{23})[1-k_{34}e^{-2mb'}+k_{12}e^{-2mb}-k_{12}k_{34}e^{-2m(b+b')}]}{1+k_{23}k_{34}e^{-2mb'}+k_{12}k_{23}e^{-2mb}+k_{12}k_{34}e^{-2m(b+b')}}. \tag{14}$$

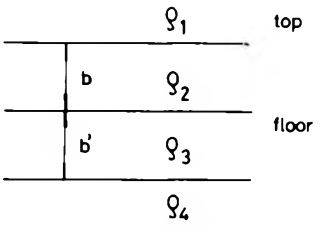

Fig. 1. Four-layer geoelectric model

1. ábra. Négyréteges geoelektromos modell

Фиг. 1. Четырехслойная модель геоэлектрической среды.

From $R'_F(m)$ the thicknesses b and b' of the coal seam and protective layer, respectively, can be expressed as

$$b = \frac{\ln \dfrac{[1-k_{23}-R'_F(m)]-[1-k_{23}+k_{23}R'_F(m)]k_{34}e^{-2mb'}}{-k_{12}[1-k_{23}-k_{23}R'_F(m)]+[1-k_{23}+R'_F(m)]k_{12}k_{34}e^{-2mb'}}}{-2m}, \quad (15)$$

$$b' = \frac{\ln \dfrac{[1-k_{23}-R'_F(m)]+[1-k_{23}-k_{23}R'_F(m)]k_{12}e^{-2mb}}{k_{34}[1-k_{23}+k_{23}R'_F(m)]+k_{34}[1-k_{23}+R'_F(m)]k_{12}e^{-2mb}}}{-2m} \quad (16)$$

5. Curve charts for $R_T(m)$ and $R_F(m)$

As has been shown, the values of $R_T(m)$ and $R_F(m)$ can be computed from Eqs. (8), (14) and (4), then they are plotted as a function of $1/m$, as illustrated in *Fig. 2a*. For the sake of comparison, *Fig. 2b* presents the corresponding specific resistivity curves of the tunnel sounding. The two kinds of curves approach the same limiting values for small AB/2 and $1/m$ values and for large AB/2 and $1/m$ values. There occurs a minor deviation between the curves at intermediate ranges (as generally realized in the VES literature).

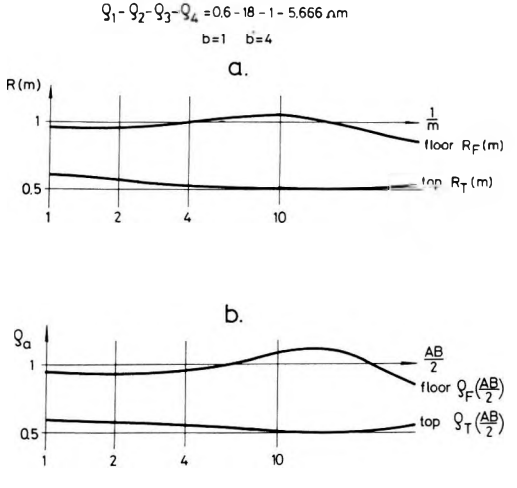

Fig. 2. Comparison of kernel functions and apparent resistivity curves of tunnel soundings
a) $R_T(m)$ and $R_F(m)$ functions
b) $\varrho_T(\mathrm{AB}/2)$ and $\varrho_F(\mathrm{AB}/2)$ functions

2. ábra. Vágatszondázások magfüggvényeinek és látszólagos ellenállás görbéinek összehasonlítása
a) $R_F(m)$ és $R_T(m)$ függvények
b) $\varrho_F(\mathrm{AB}/2)$ és $\varrho_T(\mathrm{AB}/2)$ függvények

Фиг. 2. Сопоставление подъинтегральных К-функций и кривых кажущегося сопротивления зондирований по горным выработкам.
a) Функции $R_T(m)$ и $R_F(m)$.
b) Функции $\varrho_T(AB/2)$ и $\varrho_F(AB/2)$.

The interpretation of the measured curves requires the computation of a large number of theoretical curves. However, upon transforming the measured apparent specific resistivity curves into $R(m)$ curves by means of Eq. (6), the comparsion of the curves will be much more easier in the (R/m), $1(m)$ coordinate system than in the ϱ_a, AB/2 system. Since Eqs. (8) and (14) can be programmed for small-capacity desk-top computers, the computation of $R(m)$ curves for a multilayered model of arbitrary parameters should cause no difficulties.

6. Transformation program for a desk-top calculator

The expression in Eq. (6) is substituted by the finite sum

$$R(m_k) \approx \varrho_e + \sum_{i=1}^{n} \Delta\varrho_i \int_{\frac{r_i - r_{i-1}}{2}}^{\frac{r_i + r_{i+1}}{2}} J_1(m_k r_i) \frac{dr}{r_i}, \tag{17}$$

where $\varrho_e = \varrho_{12}$ for the top sounding; $\varrho_e = \varrho_{23}$ for the floor sounding; r_i and $\Delta\varrho_i$ are the AB/2 and $\Delta\varrho(r)$ values corresponding to the equidistant points r_i of the sounding curves. The values $1/m_k$ are abscissae of the equidistant points of the kernel function. In other words, the equidistant points of the function $R(m)$ can be obtained in a logarithmic coordinate system by summing the values $\Delta\varrho_i$ (weighted by the integrals of Eq. 17) belonging to the equidistant points of $r = \mathrm{AB}/2$.

The transformation program is given in *Appendix I*, the values of the integrals in Eq. (17) are incorporated in the program.

To make the program applicable for VES measurements with greater AB/2 distances, the input values ϱ_a should be entered for the whole range AB/2 = 0.8 – – 500 m. Since there is no special branch in the transformation program for the asymptotic part of the apparent resistivity curve, the array reserved for the $\Delta\varrho$ values should be completely filled, even beyond the limits $\varrho_a = \varrho_1$ or $\varrho_a = \varrho_n$.

By applying the program to different kinds of problems, the errors due to different neglections and approximations have been found less than 2%, up to $\frac{1}{m} = 50$. For example, for the model $\varrho_1 - \varrho_2 - \varrho_3 - \varrho_4 = 0.6 - 18 - 1 - 5.666\ \Omega\mathrm{m}$; $b = 1$; $b' = 4$ the specific resistivity values of the floor sounding were transformed into a kernel function by means of the program of Appendix I. The percentage errors, proceeding in (logarithmically) equal steps from $r/b = 0.63$ to $r/b = 50$ were as follows: 0.0, 0.0, 0.0, 0.2, 0.3, 0.3, 0.2, 0.0, −0.1, −0.2, −0.3, −0.4, −0.3, −0.2, −0.2, −0.1, −0.1, −0.1, −0.3. It is expected, of course, that more significant errors would occur for a $\varrho_3 = \infty$ type VES curve.

7. Computation of the layer parameters

If the specific resistivities are known, the layer thicknesses can be determined from the transformed $R_2(m)$ values by means of Eqs. (9, 10) for top soundings, and by Eqs. (15, 16) for floor soundings. Also, the value of ϱ_3 can be expressed (Eq. 11) from the basic equation (8) of the top sounding, i.e. besides thickness, specific resistivity can be determined as well.

By applying the iteration formula

$$x_{n+1} = f(x_n),$$

where $x = (b, b')$ or, for example, $x = (b, \varrho_3)$, for some transformed $R_m(m)$ f will be given by Eqs. (9), (10) and/or (9), (11) for the top sounding, and by Eqs. (15), (16) for the floor sounding.

The equations of the top sounding can also be utilized to interpret the VES curves obtained at the surface, by substituting $\varrho_1 = \infty$ (the number of layers is decreased by one). In this case ϱ_2 becomes ϱ_1, b becomes h_1, etc. In VES the specific resistivity ϱ_2 (that was ϱ_3 in the preceding) should be determined from some characteristic part of the $R(m)$ curve, as for example, from two values of this curve where the effect of the second layer has already appeared while that of the third is still negligible, i.e. the estimated value $h_2 = b'$ will not cause too much of an error in the computation of ϱ_2 and h_1.

The programs in *Appendix II* are constructed in such a way that the initial value of b (memory location 5), appropriate values of $R(m)$ (memory locations 6, 26), the corresponding values m for $1/m$ (locations 7, 27) and the specific resistivities of the individual layers (memory locations 1, 2, 3, 4) should be entered as input parameters. For the iterative computation of ϱ_3 and b the estimated value b' (location 25) and the specific resistivities of the other layers (locations 1, 2, 4) should be specified. For the top sounding b' is computed from the $R(m)$ value corresponding to the greater $1/m$; for floor soundings from the $R(m)$ value corresponding to the smaller $1/m$; that is, memory locations 6 and 7 should contain the appropriate $R(m)$, m values. If these pairs are given in reversed order, the program will diverge, i.e. no solution (b, b', ϱ_3) will have been found. By computing the solutions for b and b' from several ($R(m)$; m) values, the deviations of these solutions give an idea about how much the $R(m)$ curve corresponds to the model assumed.

The iterative programs are contained in Appendix II. A simple example for floor sounding is given below.

Values computed for a $\varrho_1 - \varrho_2 - \varrho_3 - \varrho_4 = 0.6 - 18 - 1 - 5.666$ Ωm; $b = 1$ $b' = 4$ model (half-space geometry)

$1/m$	$R(m)$
3.18	0.944
8.02	1.0592
40.40	0.8145

Input parameters for the iterative program: ϱ_1, ϱ_2, ϱ_3, ϱ_4; two pairs of m, $R(m)$ and the initial value of b.

$\varrho_1 = 0.6\ \Omega$m		$\varrho_2 = 18\ \Omega$m	$\varrho_3 = 1\ \Omega$m		$\varrho_4 = 5.666\ \Omega$m
$1/m = 3.18$		8.02	3.18		40.4
$R(m) = 0.944$		1.059	0.944		0.8145
$b = 1.20$	initial	$b' = 4.41$	$b = 1.20$	initial	$b' = 4.41$
1.13		4.27	1.02		4.05
1.08		4.18	1.00		4.00
1.05		4.11			
$b = 0.60$	initial	$b' = 2.97$	$b = 0.60$	initial	$b' = 2.97$
0.74		3.37	0.94		3.87
0.83		3.61	0.99		3.99
0.89		3.76			
By reverse order of the $R(m)$ memories					
$b = 1.20$	initial	$b' = 4.61$			
1.31		4.89			
1.46		5.25			
1.68		5.69			

8. Conclusions

It has been shown that the interpretation of geoelectric soundings performed in mine drifts can be realized using the kernel function method on an easily available TI—59 (Texas Instruments) calculator, for models consisting of four or even more layers. For the iterative programs of the multi-layered models the kernel functions can be expressed as simple rational functions so that the layer parameters (e.g. thickness of the protective layers) can easily be determined.

REFERENCES

CSÓKÁS, J. 1980: Methodological development of the geoelectric investigation of tectonic disturbances in brown coal mines. Final Research Rept. Geophysics Dept. of University of Heavy Industry, Miskolc (in Hungarian)

GYULAI, Á. 1979: Interpretation of geoelectric soundings in coal mines. Magyar Geofizika, 20, pp. 142—148 (in Hungarian)

KOEFOED, O. 1979: Geosounding Principles, 1. Resistivity Sounding Measurements. Elsevier, Amsterdam—Oxford—New York

VAN NOSTRAND, R., COOK, K. L. 1966: Interpretation of Resistivity Data. U.S. Government Printing Office, Washington D.C.

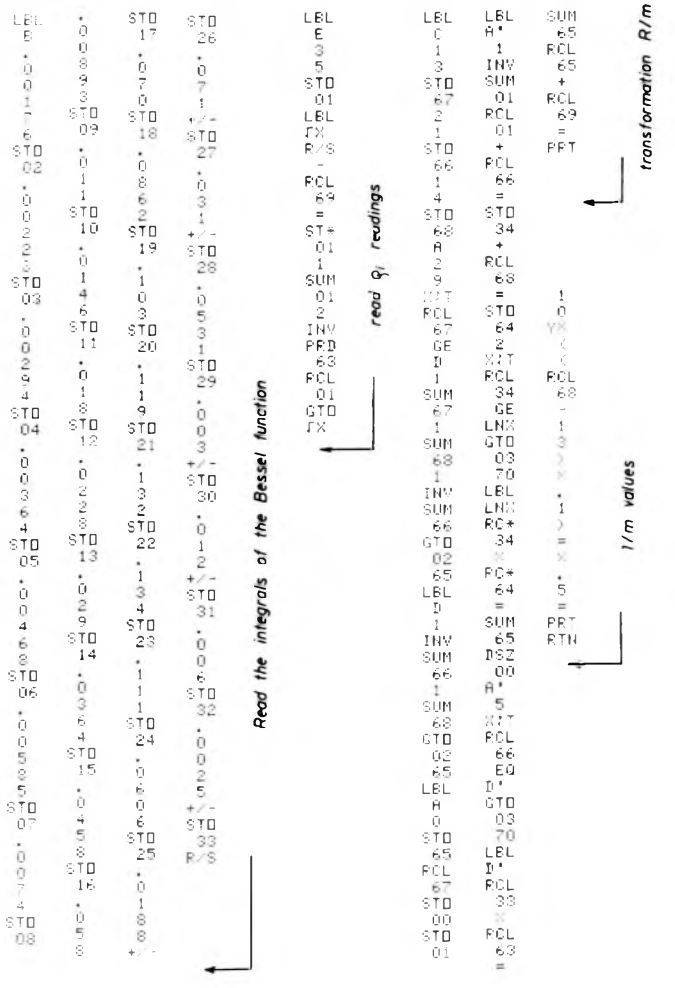

Appendix 1. The $\varrho_a \rightarrow R(m)$ transformation program for the TI—59 calculator

Function of keys:

[B] Read the integrals of the Bessel function; [E] Load ϱ_a to memory locations 35—63.

After [E], further parameters are loaded into the storage unit denoted by R/S ;

[C] Transformation $R(m)$ until $\frac{1}{m} = 0.63$ is reached, or; [A] Transformation $R(m)$ for $1/m$ values depending on the contents of storage units 66,67,68

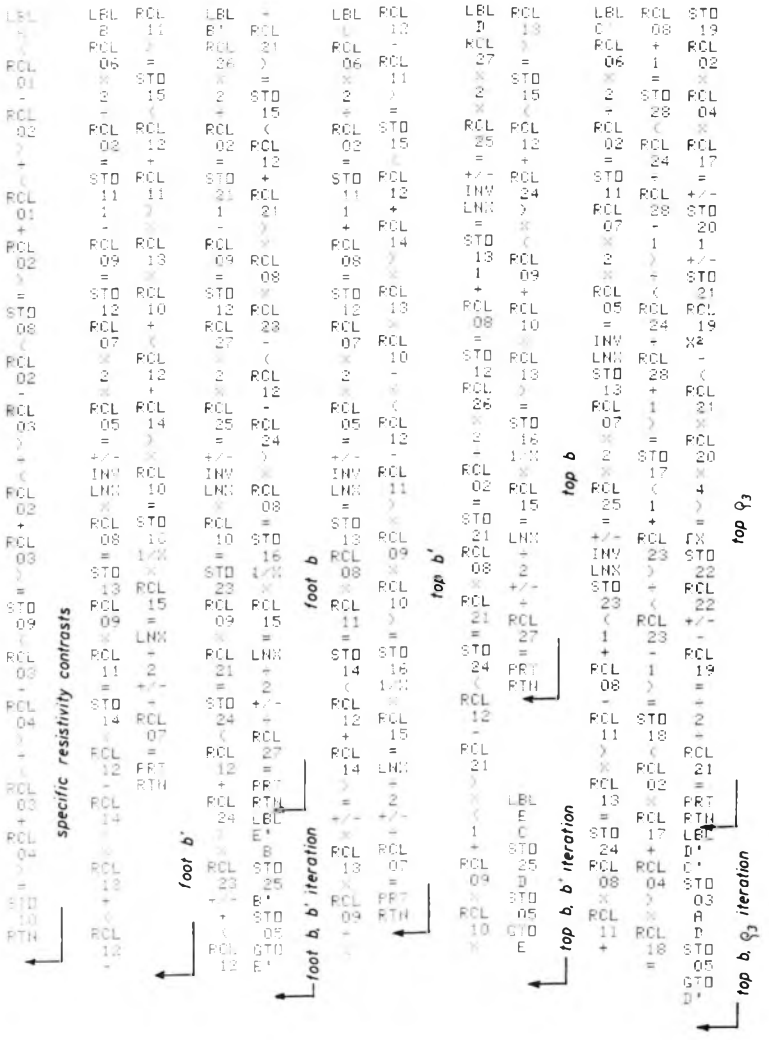

Appendix II. Programs for the TI—59 calculator for the iterative determination of the layer parameters from the $R(m)$ function

Function of keys:

[A] contrasts, [E], [E'] or [D'] iteration

GYULAI ÁKOS

GEOELEKTROMOS VÁGATSZONDÁZÁSOK KIÉRTÉKELÉSE MAGFÜGGVÉNYEKKEL

A bányatérségekben végzett geoelektromos vágatszondázások legfőbb célja, hogy telep- és védőréteg vastagság adatokat szolgáltassunk a bányaműveletek tervezéséhez. A szondázási görbék kiértékelése vagy elméleti görbékkel való összehasonlítással, vagy magfüggvény felhasználásával lehetséges. A dolgozat ez utóbbi megoldás felhasználásával kifejlesztett algoritmust és annak gyakorlati megvalósítására a TI—59 kalkulátorra írt programokat ismerteti.

А. ДЮЛАИ

ИНТЕРПРЕТАЦИЯ КРИВЫХ ЭЛЕКТРОРАЗВЕДКИ МЕТОДОМ ЗОНДИРОВАНИЯ ПО ГОРНЫМ ВЫРАБОТКАМИ С ПОМОЩЬЮ ПОДЪИНТЕГРАЛЬНЫХ К-ФУНЦИЙ

Основной целью электроразведки методом зондирования в горных выработках является представление данных по мощности промышленных пластов и залегающих в их кровле экранирующих горизонтов для проектирования горных выработок. Интерпретация кривых зондирования производится либо путем их сопоставления с теоретическими кривыми, либо с и пользованием подъинтегральных К-функций. В работе излагается алгоритм, разработанный путем реализации второй возможности, и программы для проведения расчетов с его помощью на калькуляторе TI-59.

EÖTVÖS LORÁND GEOPHYSICAL INSTITUTE OF HUNGARY
GEOPHYSICAL TRANSACTIONS 1982
28/2 pp. 57—75

NEW METHODS OF STUDYING THEORETICAL AND MODELLED NEUTRON FIELDS FOR DETERMINING NEUTRON POROSITY

L. ANDRÁSSY*, I. BARÁTH*, L. CSEREPES**

The multi-group diffusion theory was used to calculate neutron distribution for a medium consisting of a borehole and rock formation. A new method was elaborated to solve one of the most complicated questions of multi-group diffusion theory: the calculation of group constants. Four-group flux vs. porosity curve sets are calculated for one-detector and two-detector (compensated) recording systems assuming various rock matrixes, sonde lengths and borehole diameters. A discussion is given on the method created to transform modelled to theoretical neutron fields. The general form of transformation equations is described and practical applications of the method are indicated. Experimental model measurements are presented to illustrate the separation of thermal and epithermal neutron groups using filters.

1. Introduction

Calibration of the sonde in rock models is indispensable for interpreting neutron-neutron logs. The calibration measurements can, of course, embrace a narrow range of cases being encountered in actual operations, thus their theoretical extrapolation is also needed. Starting from this requirement, investigations were carried out to determine theoretically neutron distributions in boreholes on the one hand, and to transform theoretical neutron fluxes into count rates as measured by actual neutron deterctors, on the other.

2. Theoretical determination of neutron flux in boreholes

The multi-group version of the diffusion theory was used to calculate the neutron flux. The original form of the diffusion equation defines the scalar flux $F(E, r)$ continuously depending on the neutron energy E in the following manner:

$$\frac{1}{3\Sigma^{(tr)}(E)} \nabla^2 F(E, r) - \Sigma^{(t)}(E) F(E, r) + \int_0^\infty \Sigma^{(S)}(E', E) F(E', r)\, dE' + S(E, r) = 0. \tag{1}$$

* Eötvös Loránd Geophysical Institute of Hungary, Budapest
** Department of Geophysics, Eötvös Loránd University, Budapest
Paper presented at the 26th Geophysical Symposium, Leipzig, 22—25 September, 1981.

Here r is the position vector; time as a variable can be omitted in accordance with the conditions of neutron-neutron logging. $\Sigma^{(tr)}(E)$ and $\Sigma^{(t)}(E)$ are the transport and total macroscopic cross sections respectively, $\Sigma^{(S)}(E', E)$ the cross section of neutron scattering from energy E' to E. For simplicity the dependence of these cross sections on position in a heterogeneous medium is not marked. $S(E, r)$ is the source density.

Following the usual way of solving Eq. (1) the continuous energy is discretized in the n-group diffusion theory, i.e. the possible values of the neutron energy E were grouped into intervals. These intervals are given numbers according to the sequence of decreasing energy. Neutrons falling in the i-th interval (E_i', E_i'') form the i-th neutron group. Then the theory furnishes instead of the continuous $F(E, r)$ the group fluxes

$$F_i(r) = \int_{E_i'}^{E_i''} F(E, r)\, dE \qquad (i = 1, 2, \ldots, n) \tag{2}$$

The equations which determine the F_i fluxes, i.e. the equivalents of (1) for n-group, are

$$D_i \nabla^2 F_i - \Sigma_i F_i + \sum_{j=1}^{i-1} \Sigma_{ji} F_j + S_i = 0 \qquad (i = 1, 2, \ldots, n). \tag{3}$$

Here D_i is the diffusion constant of the i-th group, the macroscopic cross-section (Σ_i) characterizes the escape of neutrons from the i-th group (by absorption and elastic or inelastic back scattering into a group of lower energy), Σ_{ji} is the cross-section of back scattering from the j-th into the i-th group, S_i the source intensity of neutrons generated in the i-th group. The Σ_i, Σ_{ji} and D_i group constants are the averaged values in the i-th group of the cross-sections $\Sigma^{(t)}(E)$, $\Sigma^{s}(E', E)$ and that of $\dfrac{1}{3\Sigma^{(tr)}(E)}$ appearing in Eq. (1). (The method of their calculation is shown in Section 3.)

Equations (3) were solved for the following conditions: 1) the neutron source is a point and arranged along the borehole axis. This means that our results are suitable to interpret measurements made in the central sonde position. 2) The medium is cylindrically symmetrical in relation to the borehole axis; in the radial direction (r) it is layered, in the direction of symmetry axis (z) it is homogeneous. 3) The innermost cylindrical layer is composed of borehole fluid, i.e. the presence of the sonde was not considered in the theory, but in calibration relationships only.

For the above conditions two-group flux calculations were performed earlier [Taliianskiy et al. 1960, Allen et al. 1967]. In order to improve the accuracy of theoretical fluxes the method was extended to a group division containing an increased number of neutron groups.

If the source is located at the origin, and the above limitations for the medium geometry hold true, then as the result of the solution of the above equations the neutron fluxes within the borehole are defined in the form of the following integrals:

$$F_i^{(\text{hole})}(r, z) = \int_0^{\infty} \sum_{j=1}^{i} \{e_{ij}(\lambda) I_0(\alpha_j r) + f_{ij}(\lambda) K_0(\alpha_j r)\} \cos \lambda z \, d\lambda. \tag{4}$$

Here

I_0, K_0 are the modified Bessel functions,

$$\alpha_j^2 = \lambda^2 + (\Sigma_i^{(\text{hole})}/D_i^{(\text{hole})}),$$

$$e_{ij}(\lambda) \quad \text{and} \quad f_{ij}(\lambda) \quad (i = 1, 2, \ldots, n, \quad j = 1, 2, \ldots, i)$$

are complicated functions of the group constants D_i, Σ_i, Σ_{ji} of individual layers, as well as of the boundary and source conditions. According to the boundary conditions the neutron flux and neutron current are continuous functions on the cylindrical layer boundaries, while the source conditions for a point-type source require that one takes into account the singularity of the neutron current in the origin.

In the two-group calculations of ALLEN et al. [1967] the fluxes are determined by summing up the infinite arrays which approximate the integrals instead of using expressions like Eq. (4). For an increased number of groups, however, a quicker method is needed. Our algorithm was built up on the following two findings: 1) e_{ij} and f_{ij} can be calculated through simple recursive steps progressing according to i; 2) if we replace the expression

$$\sum_{j=1}^{i} \{e_{ij}(\lambda) I_0(\alpha_j r) + f_{ij}(\lambda) K_0(\alpha_j r)\}$$

by $\dfrac{X(\lambda)}{\lambda}$ and the $\lambda = e^u$, $z = e^{-v}$ variable exchanges are used, the integral can be transformed into a convolution of the form

$$\int_0^{\infty} \frac{X(\lambda)}{\lambda} \cos \lambda z \, d(\lambda) = \int_{-\infty}^{\infty} X(e^u) \cos [e^{-(v-u)}] \, du$$

for whose calculation the linear filter theory offers an accurate and very quick method. This has already been used in several fields of geophysics to calculate convolution type integrals [GHOSH 1971, DRAHOS and SALÁT 1973; SALÁT and DRAHOS 1975].

3. Calculation of group constants

A key question in the multi-group diffusion theory is the method of determining the initial data, the group constants D_i, Σ_i, Σ_{ji}. The dependence of group fluxes on the porosity of rocks surrounding the borehole is carried by the dependence of group constants on porosity. Therefore the group fluxes can be used for the interpretation of neutron logs only when the constants can be calculated with appropriate accuracy.

Macroscopic cross-sections which depend continuously on the energy ($\Sigma^{(tr)}(E)$, $\Sigma^{(t)}(E)$, $\Sigma^{(s)}(E', E)$) can unambiguously be calculated from the basic data of neutron physics, from the microscopic reaction cross-sections of individual elements. But how will they turn into group constants? It is well known from the literature [WEINBERG and WIGNER 1958, MURRAY 1959, TITTLE and ALLEN 1966, WILLIAMS 1966, SZATMÁRY 1971] that the group constants D_i, Σ_i, Σ_{ji} can be approximated as the following averages according to energy weighted by the flux:

$$D_i \approx \left\langle \frac{1}{3\Sigma^{(tr)}(E)} \right\rangle_i$$

$$\Sigma_{ji} \approx \left\langle \int_{E_i'}^{E_i''} \Sigma^{(s)}(E, E')\, dE' \right\rangle_j \tag{5}$$

$$\Sigma_i \approx \langle \Sigma^{(t)}(E) \rangle_i - \Sigma_{ii},$$

where the averaging for a function $f(E)$ of neutron energy is realized as follows

$$\langle f(E) \rangle_i = \frac{\int_{E_i'}^{E_i''} f(E) F(E, r)\, dE}{\int_{E_i'}^{E_i''} F(E, r)\, dE} \tag{6}$$

It is mentioned that these relationships can be simply deduced by comparing Eqs. (1) and (3) and using the definitions of group constants Eq. (2).

Two serious objections can be raised against definitions (5) and (6). One of them is that an accurate calculation of averages would require the knowledge of the flux with a continuous variable $F(E, r)$ in the heterogeneous medium to be investigated. Obviously the exact shape of it is unknown; moreover, our final purpose is restrained to the calculation later on of the discretized form of $F(E, r)$, the group fluxes $F_i(r)$—using D_i, Σ_i, Σ_{ji}—according to Eq. (4). The second difficulty is that (6) contains as a parameter the variable of position r of $F(E, r)$; that is, the averages (5) are in general more or less dependent on r, even in a homogeneous medium, thus the "group constants" obtained in this way are not constant! This is why approximation signs are written in Eq. (5).

In spite of these difficulties the above definitions were nevertheless used to calculate the group constants, even for geophysical applications [TITTLE and ALLEN 1966]. In such cases it is acceptable to make use of the assumption that the flux $F(E, r)$ is a separable function of its variables:

$$F(E, r) = F^{(1)}(E)F^{(2)}(r)$$

because then $F^{(2)}(r)$ can be eliminated from (6), and the energy spectrum $F^{(1)}(E)$ is replaced by a spectrum deduced from the theory of space-independent neutron moderation [WEINBERG and WIGNER 1958, WILLIAMS 1966, SZATMÁRY 1971].

We expect however, maximum accuracy from our multi-group calculations, thus such approximations cannot be allowed in the calculation of group constants. Exact group constants are needed and the criterion of accuracy can be as follows: one must find the group constants which lead to a minimum deviation of the calculated $F_i(r)$ group fluxes from the real flux distribution. Let us call such group constants optimum group constants. In instances when optimum group constants are used the (minimized) errors of the calculated $F_i(r)$ functions will be the consequences of the discretization of (2) and cannot be attributed to deficiences of the calculation of group constants.

In our study we have realized an algorithm which is suitable to create such an optimum assembly of group constants. For the case of pre-selected neutron groups and a given neutron source this algorithm permits one to calculate the group constants for media encountered in the practice of well logging (various borehole fluids, rocks of various compositions and porosity, etc.). The constants of a given medium are achieved so that the criterion of optimization is separately used for each medium as if the space were homogeneous and being completely filled up with it. As exact flux distribution the continuous flux $F(E, r)$ calculated from the original diffusion equation (1) was used for the given homogeneous medium for a given source. Its calculation from (1) for a homogeneous medium involves no serious difficulty, it can be realized numerically. The variable of energy is again divided into intervals, thus the multi-group procedure is again used here in principle. But now the number of groups—since we now have to deal with a homogeneous medium—may be significantly more than in the case of a heterogeneous medium. We have used 26 groups. For any practical purpose it means continuous flux determination.

To write down the defining equation of our algorithm the assembly of group constants to be calculated should be designated by the following symbols:

$$\mathbf{C} = \{D_i, \Sigma_i, \Sigma_{ji};\ i = 1, 2, \ldots, n;\ j = 1, 2, \ldots, i-1\}.$$

Group fluxes to be calculated from Eqs. (3) are functions of the matrix $\mathbf{C}$, i.e. of the variable of optimization:

$$F_i = F_i(\mathbf{C}, r)$$

Using these symbols, the criterion of optimization is

$$\sum_i \left\| F_i(\mathbf{C}, r) - \int_{E_i'}^{E_i''} F(E, r)\, dE \right\|^2 = \min_{\mathbf{C}}, \tag{7}$$

where $F_i(\mathbf{C}, r)$, $F(E, r)$ are fluxes satisfying Eqs. (3) and (1) respectively: $\min_{\mathbf{C}}$ indicates that the minimum should be searched for as a function of C. The formula determining the deviation of fluxes is given by

$$\| \Delta F_i(\mathbf{C}, r) \|^2 = \int W_i(r) [\Delta F_i(\mathbf{C}, r)]^2 \, d^3r^*,$$

where

$$\Delta F_i(\mathbf{C}, r) = F_i(\mathbf{C}, r) - \int_{E_i'}^{E_i''} F(E, r)\, dE$$

and the weight coefficient $W_i(r)$ was chosen from practical aspects, its value being high where fluxes are usually measured.

Thus the algorithm, written on the basis of minimum criterion (7) searches through the variations of group constants C for those values with which the deviation between the group fluxes and the values of the fluxes with continuous variables is reduced to a minimum. This is nothing other than a problem of minimum finding with many variables. Several excellent numeric methods are known for solving it [e.g. JACOBY et al. 1972], thus there was no difficulty in choosing among them.

4. Results of calculations

Our calculations were initially performed for two-group equations with the purpose of comparing them with results in the literature. It is practical to take the group of thermal neutrons for the group of the lowest energy (within the range 0—0.2 eV, mean energy 0.0253 eV). This is the most important neutron group; it is the energy of these neutrons that is counted by most of neutron detectors. If two neutron groups are used, the second group covers the range between 0.2 eV and the maximum encountered energy.

We give examples taken from our results with four groups. The groups are defined as follows:

1: 11.05—0.498 MeV; 2: 0.498 MeV—78.9 eV; 3: 78.9—0.2 eV the so called epithermal group; 4: 0.2—0 eV, the thermal group.

* d^3r designates volumetric integrals

The neutron detectors are practically insensitive to fluxes of the first two groups. Four-group flux vs. porosity curve sets were calculated for the following cases: the medium is composed of two layers, i.e. the borehole is surrounded by homogeneous rock; the rock material is limestone or sandstone; both borehole and pores are filled with fresh water; porosity 0—40%; borehole diameter 0—254 mm, the sonde length (source-detector spacing) varies from 300 to 900 mm. The spectrum of the source is equal to the spectrum of PuBe, though obviously the calculations can easily be performed for sources having different spectra. In *Table I* group constants calculated for a matrix of limestone are presented as an example.

In *Fig. 1* the dependence of thermal and epithermal fluxes on porosity in limestone is shown for a sonde length of $l = 400$ mm, the borehole diameter being the parameter of curves. In *Fig. 2* the same case is presented for a sandstone matrix for comparison.

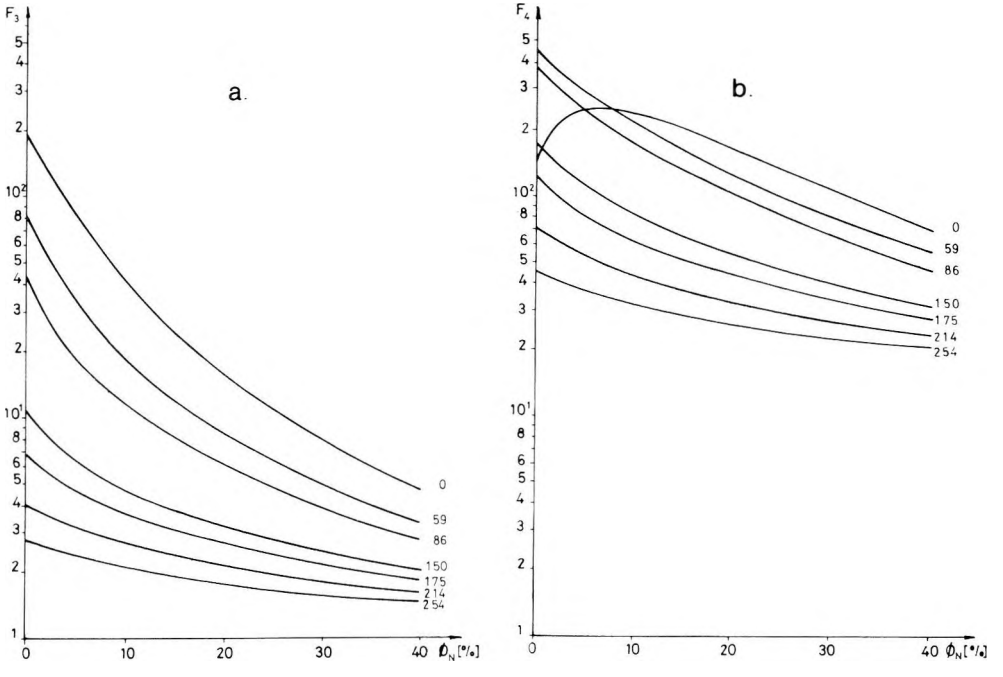

Fig. 1. Theoretical curve sets for epithermal (a) and thermal (b) neutrons. Sonde length: 400 mm, limestone matrix

1. ábra. Elméleti görbeseregek epitermikus (a) és termikus (b) neutronokra. Szondahossz: 40 cm, mészkő mátrix

Рис. 1. Теоретические палетки для надтепловых (а) и тепловых (b) нейтронов. Длина зонда: 40 см, порода: известняк.

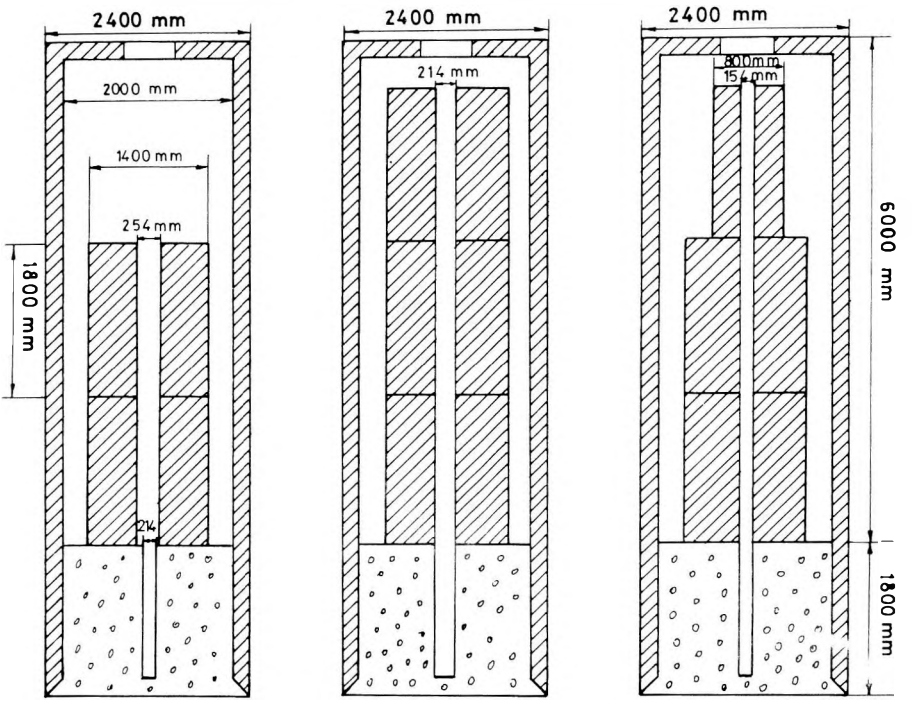

Fig. 3. Arrangement of the limestone standard array
3. ábra. Mészkő modellsor elrendezési rajza
Рис. 3. Вид распределения известняковой модельной серии.

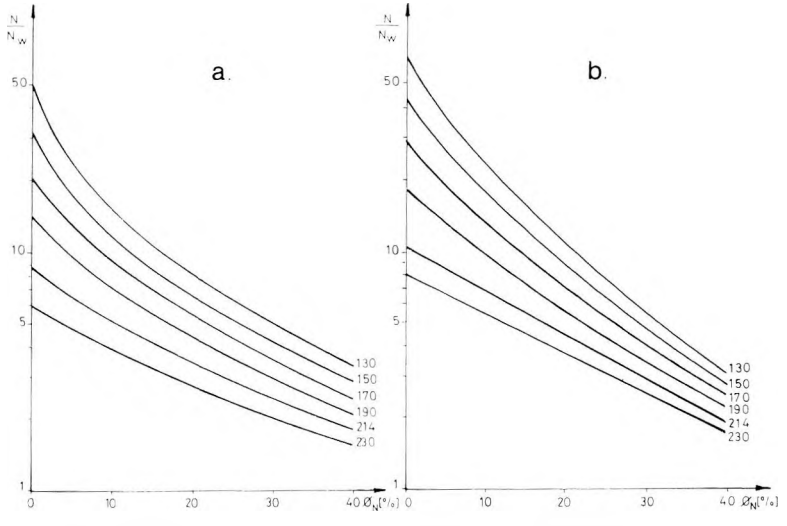

Fig. 4. Calibration curve sets for epithermal (a) and thermal (b) neutrons
4. ábra. Hitelesítő görbeseregek epitermikus (a) és termikus (b) neutronokra
Рис. 4. Калибровочные палетки для надтепловых (а) и тепловых (b) нейтронов.

6. Method used to transform modelled to calculated neutron fields

The theoretical foundation of the method was elaborated by Olgaard and Haahr in 1967. We have further developed their method and applied it to the multi-group case.

In our calculations it was assumed that apart from water the boreholes contain a point-type neutron source only. In practice, however, the sonde is also present in model- and borehole measurements leading to a distortion in the distribution of neutrons in an unknown manner. If the dependence of the neutron flux on energy and position $F(E, r)$ in the volume element dV of the neutron detector of volume V and the macroscopic cross-section of the nuclear reaction $\Sigma^{(m)}(E)$ are known, then the count value N, for the given $t = t_0$ period ($t_0 = 60$ sec) is described by the integral relationship

$$N = \int_{t_0} \int_{V} \int_{E} \Sigma^{(m)}(E) \varepsilon(E) F(E, r)\, dE\, dV\, dt, \tag{8}$$

where the integration according to the energy is continued to the maximum encountered energy.

Relation (8) can be transformed after a certain simplification of the physical conditions and rendered suitable for the comparison of fluxes calculated with the four-group theory with measured count numbers. It is assumed that the neutron flux $F(E, r)$ is independent of position within the detector and identical with the theoretical fluxes $F(E, r_0)$ calculated for the geometrical centre $r = r_0$ of the detector.

The presence of the sonde modifies the distribution of flux within the detector, reducing it significantly in relation to the theoretical value $F(E, r_0)$. This effect will be accounted for by the factor $\varepsilon(E)$.

Integral (8) comprising the energy as a continuous variable can be transformed into a sum after the group-fluxes (2) have been introduced (source intensity and detector volume taken as unit):

$$N = 60 \sum_{i=1}^{4} \varepsilon_i \int_{E_i'}^{E_i''} \Sigma^{m}(E) F(E, r_0)\, dE = 60 \sum_{i=1}^{4} \varepsilon_i \Sigma_i^{(m)} F_i(r_0), \tag{9}$$

where ε_i is the average of $\varepsilon(E)$ in the i-th group, and
$\Sigma_i^{(m)}$ is the average of $\Sigma^{(m)}$ also in the i-th group.

The factors ε_i are obtained from comparing theoretical curves with calibration measurements. The values $\Sigma_i^{(m)}$ are theoretically determined.

7. Practical solutions transforming modelled to theoretical neutron fields

Model measurements to separate thermal and epithermal neutrons

While in the four-group case the theoretical calculations approximate the spatial distribution of neutrons in a spectral way and describe it with the aid of mathematical relationships, actual logging does not permit one to distinguish the groups.

In order to separate thermal and epithermal neutron groups model measuremets were carried out using the KRNN—2—150—60sY type of sonde in the limestone standard array. The sonde was covered by Cd shields of varying thickness. As cadmium intensively absorbs neutrons with energies less than about 0.44 eV (resonance energy being 0.176 eV), it can be used to separate groups of thermal and epithermal neutrons.

Results are presented in *Figs. 5 and 6.* These figures show the relationship between counts and Cd thickness for short and long sondes, measured in the central position and with the sonde pressed against the borehole wall.

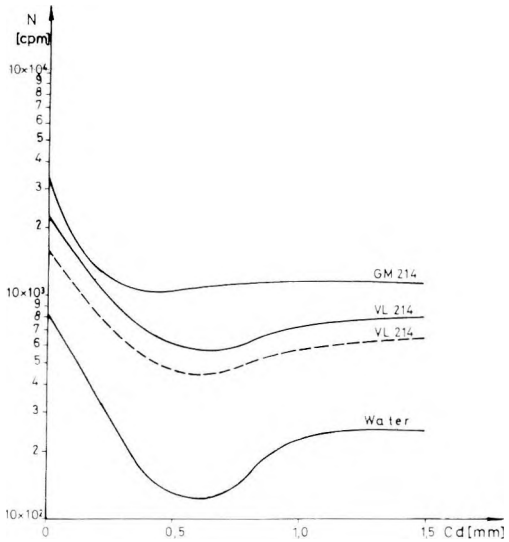

Fig. 5. Relationship between measured count number and Cd thickness with sonde in central position (continuous line) and pressed against the borehole wall (dashed line)
Sonde length: 350 mm, borehole diameter: 214 mm

5. ábra. Összefüggés a mért beütésszám és a Cd-vastagság között centrikus (folytonos vonal) és falhoz szorított (szaggatott vonal) szondahelyzetekre
szondahossz: 35 cm, fúrólyukátmérő: 214 mm

Рис. 5. Зависимость измеренных имп/мин от толщины кадмиевой пластинки для случаев: зонд в центре скважины (сплошная линия) и зонд, прижатый к стенке (пунктирная линия). Длина зонда: 35 см, диаметр скважины: 214 мм.

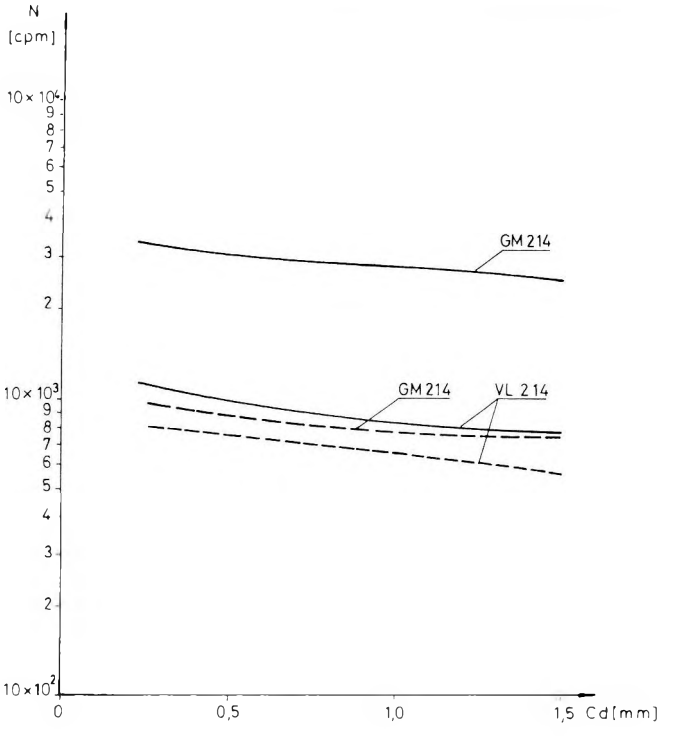

Fig. 6. Relationship between measured count number and Cd thickness with sonde in central position (continuous line) and pressed against the borehole wall (dashed line)
Sonde length: 650 mm, borehole diameter: 214 mm

6. ábra. Összefüggés a mért beütésszám és a Cd-vastagság között centrikus (folytonos vonal) és falhoz szorított (szaggatott vonal) szondahelyzetekre
szondahossz: 65 cm, fúrólyukátmérő: 214 mm

Рис. 6. То же, что и на фиг. 5., но длина зонда: 65 см, диаметр скважины: 214 мм.

Mathematical solution for transforming modelled to theoretical neutron fields for one-detector and two-detector (compensated) recording systems

As modelling conditions have been made more accurate the four-group two-layer theoretical curve sets can be modified by taking into account actual sonde parameters (sonde length, detector length and detector diameter) and source intensity.

The modified form of the theoretical curve sets for a single-detector recording system, neglecting the effect of the sonde from (9):

$$G_i(\Phi_N) = 60VQ\Sigma_i^{(m)}F_i, \tag{10}$$

$i=3, 4$ where $i=3$ for epithermal, and $i=4$ for thermal neutrons.

For compensated recording systems, relation (10) is written separately for the long and the short sonde, thermal and epithermal neutrons and the equations are divided by one another. As the result of the division the relations for the modified form of the theoretical curve sets become even simpler in such cases when the short and long detector systems are constructed in an identical way.

Our relations are as follows:

$$\Gamma_i(\Phi_N) = \frac{G_{l_i}(\Phi_N)}{G_{s_i}(\Phi_N)} = \frac{(\Sigma_i^{(m)} F_i)_l}{(\Sigma_i^{(m)} F_i)_s}. \tag{11}$$

If the detector systems are constructed in a different way the volume ratio of the long and short detectors must be accounted for in the form of a constant.

Modified theoretical curve sets for one- and two-detector recording systems are shown in *Figs. 7 and 8.*

Now the so called normal equations can be compiled for both (epithermal and thermal) groups. The normal equations establish connection between count numbers of model measurements (N_{ij}) (or the ratio of count numbers for the two-detector system $\left(\frac{N_l}{N_s}\right)_{ij}$) and the factors ε_i describing the sonde effect.

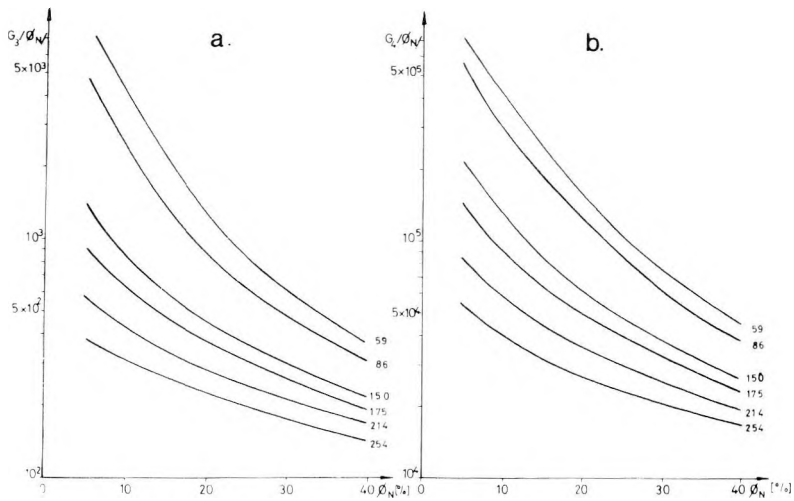

Fig. 7. Modified theoretical curve sets of single detector systems, for epithermal (a) and thermal (b) neutrons

7. ábra. Módosított elméleti görbeseregek egydetektoros rendszerre epitermikus (a) és termikus (b) neutronokra

Рис. 7. Модифицированные теоретические палетки для надтепловых (а) и тепловых (b) нейтронов в одноде текторной системе.

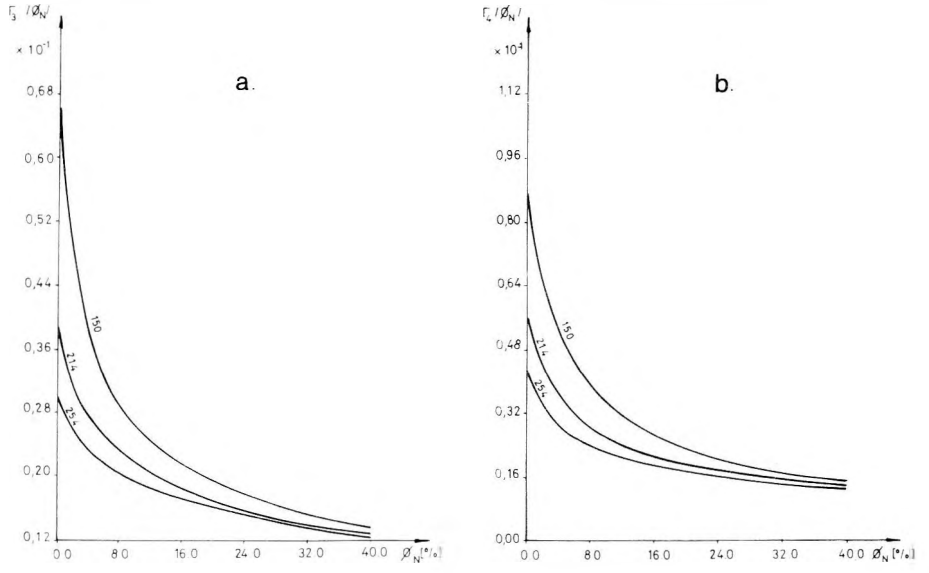

Fig. 8. Modified theoretical curve sets of two-detector (compensated) recording systems for epithermal (a) and thermal (b) neutrons
Sonde lengths: $a_s = 350$ mm; and $a_l = 650$ mm

8. ábra. Módosított elméleti görbesereg kétdetektoros (kompenzált) mérőrendszerekre epitermikus (a) és termikus (b) neutronokra
szondahosszak: $a_r = 35$ cm; és $a_h = 65$ cm

Рис. 8. Модифицированные теоретические палетки для двудетекторных (компенсированных систем для надтепловых (а) и тепловых (b) нейтронов. Длина зонда: $a_к = 35$ см и $a_д = 65$ см.

The general form of the normal equations for a single detector sonde:

$$N_{ij} = \varepsilon_i G_{ij}(\Phi_{N_j}) + \zeta_i, \tag{12}$$

for compensated recording systems:

$$\left(\frac{N_l}{N_s}\right)_{ij} = \varepsilon_i^* \Gamma_{ij}(\Phi_{N_j}) + \zeta_i^*, \tag{13}$$

where $\varepsilon_i^* = \dfrac{\varepsilon_{l_i}}{\varepsilon_{s_i}}$.

$j = 1, 2, \ldots, M$ is the serial number of calibration points.

ζ^*—is supposed to represent the effect of the sonde casing.

Eq. (13) is an approximation, but due to the low values of ζ_i^* it can be accepted and—in our experience—has proved itself adequately for practical purposes.

The values ε_i and ζ_i can be obtained from the normal equations by using the least squares method.

The transformation method is illustrated here on a practical example (*Table II*). For the normal equations (for both thermal and epithermal neutrons) the results of model measurements carried out in limestone standards of various porosities were used and the modified theoretical master curves presented in *Fig. 8* (type of sonde: KRNN—2—150—60sY two-detector, compensated system, neutron source: PuBe 5Ci, sonde in central position, $d=214$ mm). Measurement with a cadmium filter was carried out in the low porosity standard only, but results were computed for all porosity values for comparison.

The values ε_i^* and ζ_i^* as solutions of the normal equations are given in *Table III*, as well as correlation factor R. The tables show very good agreement between the orders of magnitude of theoretical and measured data.

In earlier experiments it was proved that the method cannot be used with identical ε and ζ values within the total porosity range, only between 7 and 40%. This is reaffirmed by solution B of *Table II*.

In extending the transformation method to the total porosity range we started out from the condition that at low porosities ($\Phi_N=0$—7%) in addition to H the rock matrix itself affects significantly the spatial distribution of neutron energy. Since the applied neutron detectors (N 9325) are sensitive to energy, for count numbers measured at low porosities the neutrons having higher energies than the thermal group assume an increased role. To eliminate this effect a 1 mm thick Cd shield was used for low porosities (1/a in *Table II*) ensuring the absorption of thermal neutrons. The count number received after the shield has been applied (epithermal neutrons) was deduced from the total count measured by both detectors which furnished the corrected number of thermal neutrons. The effect of shielding is very conspicuous when the correlation factors (R) are compared.

From ε_i and ζ_i calculated for borehole diameters 150 mm and 214 mm the transformation can be generalized with the aid of linear interpolation for any diameter. Transformation for any arbitrary borehole diameter ($d=150$ mm accepted as a base diameter) is provided by the following equations: for a single-detector system

$$G_i(\Phi_{N_j}) = \frac{N_{i_j} - \left[\frac{\Delta\zeta_i}{\Delta d}(d-150)+\zeta_i\right]}{\varepsilon_i - \frac{\Delta\varepsilon_i}{\Delta d}(d-150)}, \tag{14}$$

for compensated systems

$$\Gamma_i(\Phi_{N_j}) = \left\{\frac{G_l(\Phi_N)}{G_s(\Phi_N)}\right\} i_j = \frac{\left(\frac{N_l}{N_s}\right)_{i_j} - \left[\zeta_i + (d-150)\frac{\Delta\zeta_i}{\Delta d}\right]}{\varepsilon_i - \left[(d-150)\frac{\Delta\varepsilon_i}{\Delta d}\right]} \tag{15}$$

No	Φ_v %	Thermal neutrons normal equations	A	B	No	Φ_v	Epithermal neutrons normal equations	A
1.	0.28	$0.0615 = 0.0570\varepsilon_4^* + \zeta_4^*$		0.0626	1.	0.28	$0.0517 = 0.039\varepsilon_3^* + \zeta_3^*$	0.0519
1/a	0.28	$0.0954 = 0.0570\varepsilon_4^* + \zeta_4^*$	0.0952					
2.	14.86	$0.0347 = 0.0220\varepsilon_4^* + \zeta_4^*$	0.0350	0.0317	2.	14.86	$0.0295 = 0.020\varepsilon_3^* + \zeta_3^*$	0.0289
3.	16.97	$0.0339 = 0.0205\varepsilon_4^* + \zeta_4^*$	0.0325	0.0303	3.	16.97	$0.0289 = 0.019\varepsilon_3^* + \zeta_3^*$	0.0277
4.	23.13.	$0.0271 = 0.0175\varepsilon_4^* + \zeta_4^*$	0.0273	0.0276	4.	23.13	$0.0257 = 0.017\varepsilon_3^* + \zeta_3^*$	0.0252
5.	41.00	$0.0188 = 0.0130\varepsilon_4^* + \zeta_4^*$	0.0196	0.0236	5.	41.00	$0.0215 = 0.015\varepsilon_3^* + \zeta_3^*$	0.0229

Table II Normal equations for a two-detector compensated system, borehole diameter 214 mm
A – results of computation with constants determined from measurements with cadmium shield
B – results of computation with constants determined from measurements without shield

II. Táblázat Normál egyenletek kompenzált mérőrendszerre, 214 mm-es fúrólyukátmérő esetén
A – számítási eredmény a szűrővel végzett mérésből meghatározott konstansokkal
B – számítási eredmény a szűrő nélkül végzett mérésekből meghatározott konstansokkal

Табл. II. Нормированные уравнения для компенсированных измерительных систем в случае скважин диаметром 214 мм
А – расчетные данные, полученные с использованием констант, определенных по данным измерений с фильтром
В – расчетные данные, полученные с использованием констант, определенных по данным измерений без фильтра

The values ε_i and ζ_i refer to the base diameter of $d = 150$ mm.

After determining $G_i(\Phi_N)$ or $\Gamma_i(\Phi_N)$ and knowing the borehole diameter, the neutron porosity values (Φ_N) can be determined by the theoretical curve sets. theoretical curve sets.

	For thermal neutrons		For epithermal neutrons
	A	B	A
R	0.99961	0.9766	0.99658
ε_i^*	1.71905	0.8862	1.20798
ζ_i^*	−0.00279	0.01215	0.00488

Table III
III. Táblázat
Tab. III

REFERENCES

Andrássy, L., Baráth, I., Drahos, D. 1971: Homokos tárolók porozitásának meghatározása kettős forrás-detektor távolsággal végzett termikus neutron szelvényezési eljárással. Magyar Geofizika, **12,** 2—3, 63—70.

Allen, L. S., Tittle, C. W., Mills, W. R. and Caldwell, R. L. 1967: Dual-spaced neutron logging for porosity. Geophysics, **32,** 1, 60—68.

Drahos, D., Salát, P. 1973: Applications of the linear filter theory in the direct and indirect interpretation of geoelectrical and well log measurements. Annales Univ. Sci. Budapest. de R. Eötvös nominate. Sectio Geologica, **XVII,** 133.

Ghosh, D. P. 1971: The application of linear filter theory to the direct interpretation of geoelectrical resistivity sounding measurements. Geophysical Prospecting, **19,** 2, 192—217.

Jacoby, S. L. S., Kowalik, J. S., Pizzo, J. T. 1972: Iterative methods for nonlinear optimization problems. Prentice-Hall. Englewood Cliffs, New Jersey.

Murray, R. L. 1959: Nuclear reactor physics. MacMillan. London.

Olgaard, P. L., Haahr, V. 1967: Comparative experimental and theoretical investigations of the DM neutron moisture probe. Nucl. Eng. Design **5,** 311.

Salát P., Drahos D. 1975: A felszíni és karotázs elektromágneses szondázások interpretációjának az információelméleten és a lineáris rendszerek elméletén alapuló stratégiája. Magyar Geofizika **16,** 1, 14—26.

Szatmary Z. 1971: Neutrongáz-fizika. In: Neutronfizika, szerk. Kiss D., Quittner P. Akadémiai Kiadó, Budapest.

Talianskiy, I. L., Bilenkiy, B. F., Dragan, J. P. 1960: Contributions to the theory of neutron logging. Prikl. Geofizika **25,** 223—233. (in Russian)

Tittle, C. W., Allen, L. S. 1966: Theory of neutron logging II. Geophysics, **31,** 1, 214—224.

Weinberg, A. M., Wigner, E. P. 1958: The theory of neutron chain reactors. The University of Chicago Press, Chicago.

Williams, M. M. R. 1966: The slowing down and thermalization of neutrons. North-Holland, Amsterdam.

ANDRÁSSY LÁSZLÓ, BARÁTH ISTVÁN, CSEREPES LÁSZLÓ

ELMÉLETI ÉS MODELLEZETT NEUTRONTEREK VIZSGÁLATÁNAK ÚJ MÓDSZEREI A NEUTRONPOROZITÁS MEGHATÁROZÁSÁRA

A szerzők több csoportos diffúziós elmélettel számították a neutroneloszlást, fúrólyukból és kőzetformációból álló közegre. Új eljárást dolgoztak ki a több csoportos diffúziós elmélet egyik legbonyolultabb kérdésére: a csoportállandók számítására. Négycsoportos fluxus—porozitás görbeseregeket számítottak ki egydetektoros és kétdetektoros (kompenzált) mérőrendszerekre, különböző kőzetmátrixok, szondahosszak és fúrólyukátmérők esetére. A tanulmány ismerteti a modellezett neutronterek elméleti neutronterekre való átszámítására kidolgozott eljárást. Leírja az elméleti számítások és modellezések közötti transzformációs egyenletek általános alakját és rámutat az eljárás alkalmazásának gyakorlati lehetőségeire. Kísérleti modellméréseket mutat be termikus és epitermikus neutroncsoportok szűrők segítségével történő szétválasztására.

Л. АНДРАШИ, И. БАРАТ, Л. ЧЕРЕПЕШ

НОВЫЕ МЕТОДЫ ИЗУЧЕНИЯ ТЕОРЕТИЧЕСКИХ И СМОДЕЛИРОВАННЫХ НЕЙТРОННЫХ ПОЛЕЙ С ЦЕЛЬЮ ОПРЕДЕЛЕНИЯ НЕЙТРОННОЙ ПОРИСТОСТИ

На базе теории многогрупповой диффузии рассчитано распределение нейтронов в среде, состоящей из скважины и вмещающих пород. Разработана новая методика расчета групповых констант, представляющего одну из наиболее сложных проблем теории многогрупповой диффузии. Рассчитаны четырехгрупповые палетки кривых соотношения потока нейтронов с пористостью для однодетекторных и двудетекторных (компенсированных) измерительных систем, для случаев с разными породами, с различными длинами зондов и с различными диаметрами скважин. В работе излагается новый способ пересчета смоделированных нейтронных полей в теоретические нейтронные поля. Описывается общий вид уравнений трансформации, связывающих теоретические расчеты с моделированием, указываются также и практические возможности применения нового способа. Представляются результаты модельных измерений по разделению групп тепловых и надтепловых нейтронов с помощью фильтров.

EÖTVÖS LORÁND GEOPHYSICAL INSTITUTE OF HUNGARY
GEOPHYSICAL TRANSACTIONS 1982
28/2 pp. 77—87

MICROCOMPUTER CONTROLLED GEOPHYSICAL WELL LOGGING AND EXPRESS-PROCESSING SYSTEM

GY. JOSEPOVITS*, I. PÁKOZDI*, G. SZONGOTH*

The technical system of an up-to-date logger developed in ELGI and the basic principles of its operation are discussed. A special program language "KAROLIN" is described and illustrated by way of examples. Several logs recorded by the discussed well logging equipment are presented.

1. Introduction

The purpose of computerized loggers with express processing systems is to render measurement and data recording simpler and more reliable, moreover to furnish comprehensive diagrams on the results of processing to geophysicists and geologists.

Loggers are computerized in order to solve one or more of the following tasks:

a. Controlling individual logging operations.
In this case the complex well logging station is built up of several independent microprocessor controlled instruments. Each of them directs a single kind of measurement, e.g. current regulation for focused resistivity log calibration of spectral nuclear measurements and energy-stabilization of spectra, recognition of phase skips and introduction of corrections in sonic logging.
b. Controlling the integrated measuring procedure.
Maintaining data transfer to surface units, to the depth recording system, and output peripherals (display, camera, magnetic tape stores, etc).
c. Preprocessing of logs. Correlation of logs according to common depth references, calibrations, corrections and simple calculations simultaneously to logging.

The logger developed by ELGI has essentially solved tasks b and c, the complete automatic operation of the surface units, however, has not yet been realized.

* Eötvös Loránd Geophysical Institute of Hungary, Budapest
Paper presented at the 26th Geophysical Symposium, Leipzig, 22—25. Sept. 1981.

2. Construction and operation of the system

The block-diagram of the logging and express processing system is shown in *Fig. 1*. The system consists of the microcomputer and the attached peripherals. Having become familiar with the tasks and mutual relationships of the indicated units, we shall obtain a comprehensive idea of its operation, too.

Information of various downhole devices is sampled versus depth or time. Movement of the device is sensed by the depth recorder through an optical transducer attached to the measuring sheave. This unit stores depth data, visualizes the actual depth and speed for the cable guide; controls film transport in the camera and transmits periodically the depth values into the microcomputer. Depth values are corrected with the aid of magnetic markers written on the armoured cable. Automatic writing and reading of markers on the cable is executed by the surface unit, corrections for the depth values are introduced however, by the microcomputer. For measurements against time it is essential to have a timing peripheral that can be started, stopped and read by the microcomputer.

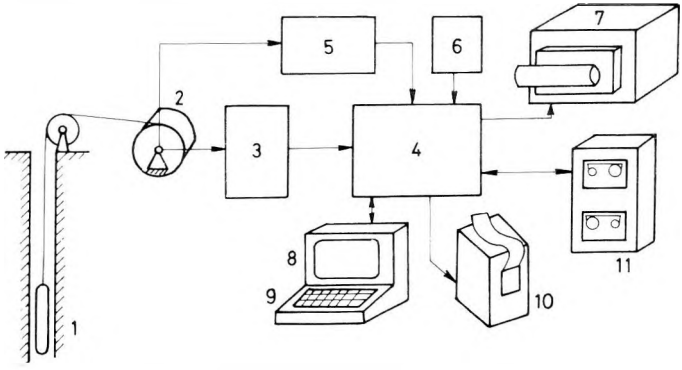

Fig. 1. Block-diagram of the logger system
1 — sonde; 2 — winch, measuring sheave; 3 — surface panels; 4 — microcomputer; 5 — optical transducer and depth recorder; 6 — timer; 7 — camera; 8 — display; 9 — keyboard; 10 — printer; 11 — magnetic cassette tape store

1. ábra. A karotázs állomás felépítésének blokkvázlata
1 — szonda; 2 — csörlő, mérőkerék; 3 — felszíni egység; 4 — mikrogép; 5 — optikai átalakító és mélységmérő; 6 — időmérő; 7 — fotoregisztráló; 8 — képernyő; 9 — billentyűzet; 10 — nyomtató; 11 — kazettás tároló

Рис. 1. Блок-схема строения каротажной станции.
1 — зонд; 2 — лебедка, измерительный диск; 3 — установка на поверхности; 4 — микро-ЭВМ; 5 — оптический преобразователь и счетчик глубины; 6 — таймер; 7 — фоторегистратор; 8 — экран; 9 — клавиатура; 10 — печатающее устройство; 11 — кассетная память.

The surface units supply power for the downhole tools and transmit their output signals to the analog-digital converter. Nine logs at most can be recorded simultaneously in digital form. Logs furnished by various sondes are related to a common depth point by the microcomputer regardless of whether they were measured in one or several runs. Two magnetic tape stores are used for correlat-

ing logs recorded in different runs. One of them provides data of logs recorded in previous runs, the other records them simultaneously together with data being measured and calculated in the present run.

The camera and the CRT display visualize measured and calculated logs arranged according to depth. Nine galvanometers of the camera perform recording in two bands of the film corresponding to API standards. Scaling according to amplitude can be divided linearly and logarithmically. The film is highlighted by applying depth numbers and grid. Logging rate is indicated by a time marker on the film. The CRT display permits one to visualize the last 25 m long sections of four logs at most. The newly recorded or calculated points of the diagrams enter synchronously with sonde movement at the top of the screen and after the cable moves a distance of 25 m they leave the screen at its bottom. Thus the operator is able to have a comprehensive view of strata penetrated by the borehole even before the film is developed. Interactive interference is also possible in the course of interpretation with the aid of a movable light-point (cursor) to be shifted over the screen.

The commands for logging and processing can be entered in the form of dialogue using a keyboard. This dialogue can be recorded on magnetic tape or burnt in a ROM resulting in a significant shortening of specification at actual logging.

It is planned to document subsequent measurement and processing with the aid of a printer.

Instead of listing technical data of the type K—20 well logging station in detail, brief information of nuclear logging should be given here to provide the reader with a notion of possibilities hidden in digital measurement techniques.

Pulses of sondes working in detector or spectral modes are handled by the equipment in the same way as regards the techniques of measurement. The equipment contains no ratemeters, the 128 channel pulse height analysis is always performed. Four energy widows of the spectrum can be selected at the operator's discretion for recording a log versus depth. Statistical scattering of nuclear measurements is reduced by digital filtering which provides symmetrical character for the beds and better resolution compared with the use of ratemeters. The filter function is available as a subprogram stored in advance in the Read Only Memory, its operation can be actuated by a single command.

The whole spectrum can be visualized on the display and recorded on the cassette-type magnetic tape together with diagrams defined by the energy windows.

3. The algorithm of express-interpretation

The operation of the microcomputer controlled logging and express processing system involves the cyclical performance of the following activities:

- performing the measurement at the n-th depth point,
- reading in from cassette data belonging to the n-th depth point but stemming from earlier measurements,
- processing data belonging to the n-th depth point,
- writing out data belonging to the n-th depth point.

In the course of operation these activites are performed for each sampling point in the above indicated succession. Thus, the system may contain simultaneously the values of all measured and processed logs that belong to a given depth point.

In the course of processing the following tasks can be solved: filtering of logs; comparing the values of two or more logs; introducing corrections into any of the logs according to a function or eventually against the values of another log; classifying the formal characteristics of logs; determining rock physical parameters from one or more logs. All these algorithms are characterized by their common feature of being performed simultaneously with the measurement and of requiring a rather limited environment of the measured point.

Processing can be imagined as a "window" sliding slowly—according to the rate of logging—over borehole data with only the data in the window being known.

A special program language for formulating the algorithm of express-interpretation has been developed in ELGI. This was necessary for adapting the algorithm of interpretation or part of it to the ad hoc requirements and the programs to the actual tasks.

A fundamental characteristic of this program language (KAROLIN) is simplicity in operation, since neither the operator conducting logging nor the geophysicist working at headquarters is in general a specialist in computation techniques.

It can be observed that programs, e.g. in FORTRAN, compiled for processing of well logs contain in 75—80% of their volumes formulae describing not the geophysical idea itself, but other instructions and commands indifferent to geophysics but indispensable in FORTRAN programming: declarations, attribution of initial values, cycle organization, data output/input commands, control transfers, etc.

In the program language KAROLIN [PÁKOZDI 1980] the instructions and commands have been implemented in such a way as to meet the special requirements of log processing. The geophysicist who writes the program should concern himself solely with the description of the relationship fundamental for geophysical interpretation. Programming of geophysical relationships has been significantly facilitated by making the logs as "log-type variables" directly accessible to any instruction: for instance, the subtraction of two depth corrected logs can be prescribed by the expression S3:=S1−S2.

4. Computer aided interpretation

There are three possibilities for data processing:

- simultaneously to measurement (using actual data and those of former runs),
- after completing the measurements, but still at the well site,
- in a computing centre.

Each stage of processing has its peculiar scope of tasks superposed in stacks. Operations to be performed simultaneously to measurement:

— correction of reference points (e.g. in electric measurements using the Gulf-Coast sonde the following four parameters are simultaneously recorded: R_{40}, R_{160}, R_{GR}, PS, with the following deviations in reference points: 0, −20, 40, 0 cm),
— conversion into physical units on the basis of calibration (e.g. °C for temperature measurements),
— dead time corrections,
— pulse number corrections using field calibrator data,
— various corrections according to drilling parameters (e.g. mud density, casing) or previously recorded logs (e.g. borehole diameter, mud resistivity, borehole temperature),
— computations on the basis of algorithms and master curves (e.g. density calculation, spectrum stripping),
— scaling according to the requirements of various presentations (e.g. logarithmic plots of electric measurements).

As a result of all these operations continuously corrected logs are obtained, arranged side by side according to depth (e.g. true resistivity, density, porosity). In addition, there is a possibility to reveal boundaries of raw material deposits (e.g. coal, bauxite, ores) from given criteria. Such marking can be made on a numeric display or on printer, and a special boundary diagram can be recorded on cassette and visualized on the camera *(Fig. 2)*.

The second stage of processing follows the completion of measurements. This stage leads to an approximate determination of quality parameters (e.g. ash content, Al_2O_3%) within the pay intervals marked off previously. Laboratory analysis results of cores and local geological conditions have to be known for the calculation of quality parameters. Of course, only relatively simple tasks (with reduced memory and time) can be performed in the field.

Resultant logs obtained in the first two stages of field interpretation are visualized on the camera and recorded on magnetic tape for further processing. All logs can be plotted in arbitrarily composed groups and to any scale (e.g. density, porosity, magnetic susceptibility, true resistivity, per cent values of K, U and Th, borehole volume). There is also a facility to plot the most characteristic logs side by side in a scale of 1 :500 or 1 :1000 in order to have a comprehensive view of the complete hole.

For the third stage of processing, in a computing centre data are entered with the aid of a data input interface or magnetic tape converter.

At the present phase of development a so called preprocessing program package has been compiled containing the following programs:

— calculation of true resistivity from three-electrode focused resistivity with corrections for borehole diameter and mud resistivity,
— calculation of the intensity of natural gamma radiation taking into consideration borehole data (borehole diameter, mud density, thickness of casing, dry hole, etc.),

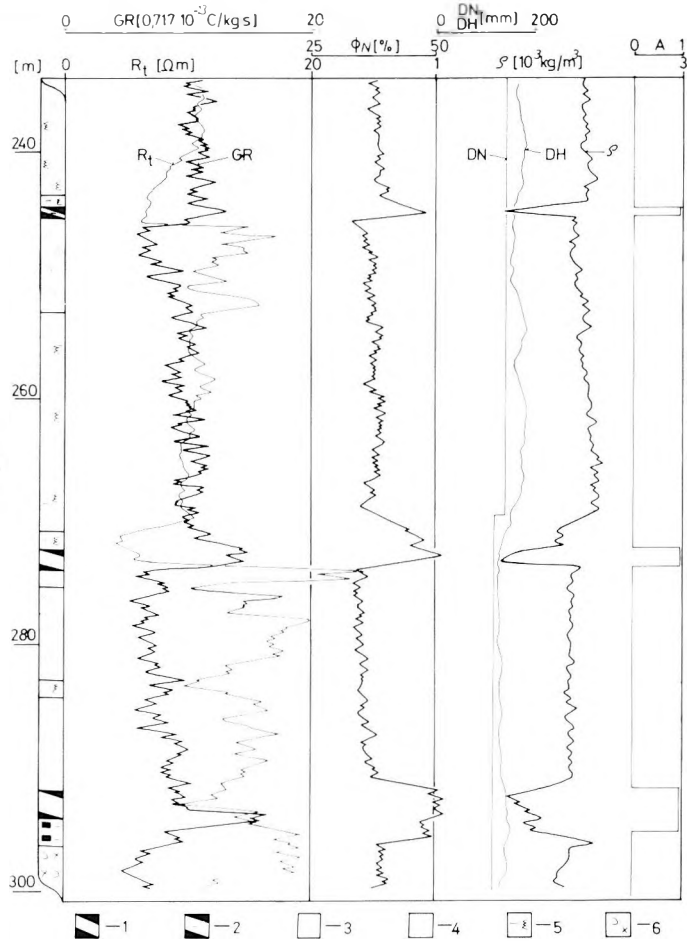

Fig. 2. Logging in a coal exploration hole

A — coal seams, determined automatically; *DH* — caliper log; *DN* — nominal borehole diameter; ϱ — density log; Φ_N — neutron porosity log; *GR* — gamma ray log; R_t — true resistivity log

1 — coal; 2 — carbonaceous clay; 3 — sand; 4 — sandstone; 5 — aleurite; 6 — rhyolite tuff

2. ábra. Kőszénkutató fúrásban végzett karotázs mérés

A — kőszenes réteg automatikus kijelölése; *DH* — lyukbőség; *DN* — névleges lyukátmérő; ϱ — sűrűség; Φ_N — neutronporozitás; *GR* — természetes gamma; R_t — valódi ellenállás

1 — szén; 2 — szenes agyag; 3 — homok; 4 — homokkő; 5 — aleurit; 6 — riolit tufa

Рис. 2. Каротажные измерения в скважине на уголь.

A — автоматическое выделение угольного пласта; *DH* — диаметр скважины; *DN* — номинальный диаметр скважины; ϱ — плотность; Φ_N — нейтронная пористость; *GR* — интенсивность естественного гамма-излучения; R_t — истинное сопротивление.

1 — уголь, 2 — углистые глины, 3 — пески, 4 — песчаники, 5 — алевролиты, 6 — риолитовые туфы.

- density calculation from gamma-gamma measurement taking into account borehole data,
- calculation of sonic velocity log,
- calculation of porosity from neutron-neutron measurement with correction for borehole diameter,
- calculation of resistivity from induction measurement,
- calibration and scaling of borehole diameter,
- calculation of percentage K, U and Th concent from energy-selective natural gamma measurement (by the method of stripping) taking into account borehole data.

Of the programs we present first an algorithm to correct the gamma ray log and the program written in KAROLIN language:

$$GR = N_{TG}\frac{N_H}{N'_H}\frac{1}{\mathrm{K}}10^{0.000774\cdot\begin{cases}(DH-D_s)\varrho_m & \text{no casing}\\ (ID_c-D_s)\varrho_m+23.9d_c & \text{with casing}\end{cases}}$$

			symbols in program language
where	GR	calculated intensity of natural gamma radiation [C/kgs]	S6
	N_{TG}	measured count number [cpm]	S4
	N_H, N'_H	counts measured by the field calibrator during calibration and measurement respectively [cpm]	K4, K5
	K	sonde sensitivity [cpm/C/kgs]	K3
	DH	measured borehole diameter [mm]	S2
	D_s	sonde diameter [mm]	K1
	ϱ_m	mud density [10^3 kg/m^3]	K2
	ID_c	inner diameter of casing [mm]	K7
	d_c	casing thickness [mm]	K6
		actual depth	M
		casing shoe depth	K10
		fluid level depth	K11

Borehole data needed in calculations are written in the corresponding memory sections prior to measurement, caliper data are recorded on magnetic tape and played back simultaneously to measurement. In the course of its work the program automatically changes over at the casing shoe or mud-air boundary to the corresponding algorithm and performs subsequent calculations with it.

Computer program in KAROLIN language (multiplication marked by *):

```
K12: K4/(K5*K3)
K18: (K7−K1)
K13: K18/(K8−K1)
K14: 3.27−K13
K19: K14*K18
K15: K19*K2/2.27
K16: 23.9*K6
K17: K8−K7+K16
K20: 10!774E−6
IND
K22: (S2−K1)*K2          no casing, with mud
K27: M>K11
K22: K22*K27             no casing, dry hole
K25: K10>M
IF(K25)                  with casing, with mud
K22: K17*K15
K26: K11>M
IF(K26)                  with casing, dry hole
K22: K17
EF
EF
K28: K20!K22
K29: K28*K12*60
S6: F1(S4)*K29           calculated gamma ray intensity
END
```

K17 through K29 are working variables, S-s are measured or calculated logs, F1(S) is a special filter function to smooth radioactive logs. Between IND and END the calculations are performed in each cycle, between IF and EF in such instances only when the value of the logical variable belonging to IF is 1.

Our second example illustrates the interpretation of a three-electrode focused resistivity log (LL3) where borehole diameter and mud resistivity are taken into account. The algorithm is as follows:

$$R_t = \frac{1.88 \frac{V}{I} SK - \left(\lg \frac{DH}{4.25}\right) R_m}{\lg \frac{3400}{DH}},$$

			symbols in program language
where	R_t	calculated true resistivity [Ωm]	S5, S6
	V	measured voltage [V]	S3
	I	measured current [mA]	S4
	DH	measured borehole diameter [mm]	S1
	R_m	measured mud resistivity [Ωm]	S2
	SK	scale factor	K1

Program in KAROLIN language:

```
K1: 50
IND
K2: (S3/S4)*K2*1.88
K3: S1/42.5
K4: LG(K3)*S1
K5: 3400/S1
K6: LG(K5)
S5: (K2−K4)K6          Rt
K7: LG(S5)*315
S6: K7−94.5            lg Rt
END
```

To illustrate the measurement a log recorded in a coal exploration hole with the microcomputer controlled equipment is shown in *Fig. 2.* Simultaneously to density calculation the boundaries of the coal beds are marked off on a galvanometer on the basis of a density criterion defined in advance:

$$\varrho < 1.8 \times 10^3 \quad \text{kg/m}^3.$$

Our second example shows the spectral investigation of natural gamma radiation in a bauxite exploration hole *(Fig. 3).* The percentage ratio of K, U and Th is calculated by the method of stripping from count numbers measured in the K, U and Th windows. It can readily be seen on the U curve that the radioactivity of clay underlying the bauxite (I) is due to enriched uranium rather than to thorium as in the bauxite bed.

5. Conclusions

Development of the KD—20 well logging station has been carried out within the framework of a CMEA agreement for international scientific cooperation. Apart from a great number of test measurements in Hungary a successful international approbation was held in Hungary in 1980 and demonstrations followed abroad: Czechoslovakia, 1980 for ore; Soviet Union, 1981 for coal; Bulgaria, 1982, for uranium.

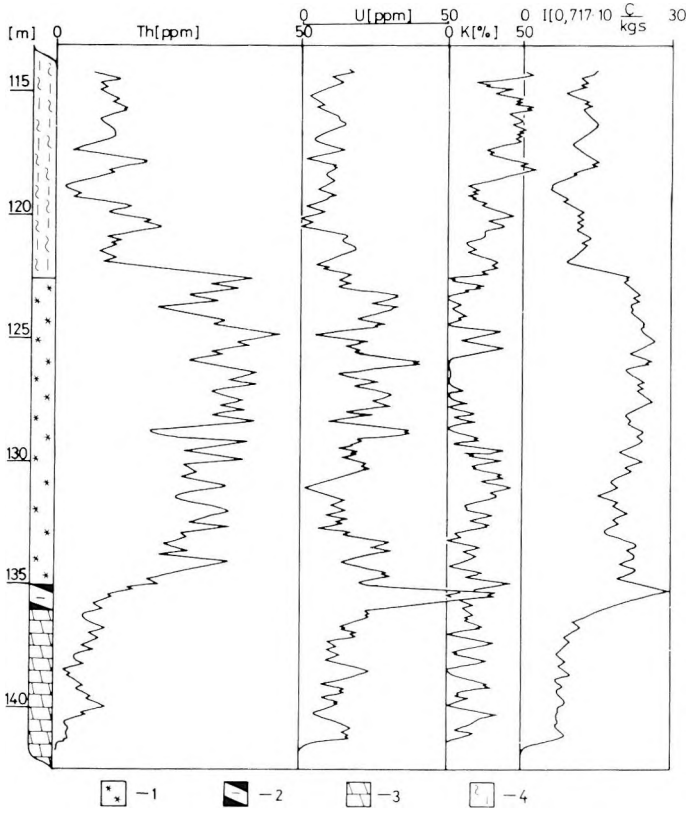

Fig. 3. Spectral investigation of natural gamma radiation in a bauxite exploration hole
1 — bauxite; 2 — carbonaceous clay; 3 — dolomite; 4 — marl

3. ábra. A természetes gamma-sugárzás spektrális vizsgálata bauxitkutató fúrásban
1 — bauxit; 2 — szenes agyag; 3 — dolomit; 4 — márga

Рис. 3. Спектральное изучение естественного гамма-излучения в скважине на бокситы.
1 — бокситы, 2 — углистые глины, 3 — доломиты, 4 — мергели

REFERENCES

PÁKOZDI, I. 1980: Dedicated computer language for a special purpose microcomputer system. Proceedings of MIMI '80 Conference, Budapest, 1980. Sept. 9—11, pp. 93—97.

JOSEPOVITS GYULA, PÁKOZDI IMRE, SZONGOTH GÁBOR

MIKROSZÁMÍTÓGÉPPEL VEZÉRELT MÉLYFÚRÁSI GEOFIZIKAI MÉRŐ- ÉS GYORSKIÉRTÉKELŐ RENDSZER

A tanulmányban a szerzők ismertetik az ELGI-ben kifejlesztett korszerű mélyfúrásgeofizikai eszköz rendszertechnikai felépítését, működésének alapelvét. Ismertetik és példákon keresztül bemutatják a speciális KAROLIN programnyelvet. Bemutatnak néhány szelvényt, amelyeket az ismertetett karotázs berendezéssel készítettek.

Л. ПОЗЕПОВИЧ, И. ПАКОЗДЫ, Г. СОНГОТ

КОМПЬЮТИЗИРОВАННАЯ СИСТЕМА ДЛЯ ИЗМЕРЕНИЯ И ЭКСПРЕСС-ОБРАБОТКИ КАРОТАЖНЫХ ДАННЫХ

В работе изложены техническая система разработанной в ЭЛГИ современной каротажной аппаратуры, принципы ее работы. Дается описание специального программного языка «КАРОЛИН», который иллюстрируется на примерах. Приводятся некоторые диаграммы, которые были изготовлены при помощи указанной каротажной аппаратуры.

EUROPEAN ASSOCIATION OF SCIENCE EDITORS

Press Release

NEW ASSOCIATION OF SCIENCE EDITORS

A new association of science editors was founded on 14 May. The European Association of Science Editors, EASE, is the result of a merger at their conference in Pau, France, between the former European Life Science Editors' Association (ELSE) and the European Association of Earth Science Editors (EDITERRA).

Besides continuing publication of *Earth & Life Science Editing* every four months, the new association will expand its programme of regular conferences and workshops. The next workshop will be held in York on 4–5 November 1982; it is hoped to have a further workshop in 1983; and there will be a joint conference with the Council of Biology Editors at Trinity College, Cambridge, in September 1984. Membership is open to all editors and those working in the dissemination of scientific knowledge.

The first President of EASE is Dr Stephen Lock, Editor, *British Medical Journal*, and the Vice-President Professor Paul Fogelberg, of the University of Helsinki, who is editor of Boreas. Further information may be obtained from the Secretary/Treasurer, Miss Nancy Morris, PO Box 33, Farnham, Surrey, GU10 3JX, UK (Tel.: 0252 723945).

Készült a Prospektagent Gmk. gondozásában,
Szedte a Nyomdaipari Fényszedő Üzem 829225/9
Budapesti Fényszöv 82-549